Standard Title Page - Report on State Project

Report No.	Report Date	No. Pages	Type Report: Final	Project No.: 70298
VTRC 06-CR9	December 2005	72	Period Covered: 08/15/2003 – 12/15/2005	Contract No.

Title: Development of Nondestructive Methods for Measurement of Slab Thickness and Modulus of Rupture in Concrete Pavements

Key Words: Nondestructive testing, Slab thickness, Modulus of Rupture, Impact Echo

Authors: John S. Popovics, Ph.D., P.E., Alex Gibson, Ph.D., and Gonzalo Gallo

Performing Organization Name and Address:

Virginia Transportation Research Council
530 Edgemont Road
Charlottesville, VA 22903

Sponsoring Agencies' Name and Address

Virginia Department of Transportation
1401 E. Broad Street
Richmond, VA 23219

Supplementary Notes

Abstract

This report describes work to develop non-destructive testing methods for concrete pavements. Two methods, for pavement thickness and in-place strength estimation, respectively, were developed and evaluated. The thickness estimation method is based on a new hybrid approach that combines frequency domain (impact-echo) and time domain (seismic) data. This new method makes use of a fuller understanding of the dynamic wave phenomenon, which was developed during the course of the work. The effects of material property gradients (due to aggregate segregation and moisture variation) through the slab thickness are compensated for in the method. A field testing method is proposed, described, and experimentally verified. Verification tests carried out on full-scale concrete slabs cast on granular base show that the new method provides more accurate thickness estimates than those obtained by the standard impact-echo procedure. On average, the error between predicted thickness and actual thickness determined by cores is less than 6 mm, although some individual estimates exceed this error value. However, the new method does not work on concrete over asphalt or cement-treated base (which accounts for most concrete pavements) or on full-depth asphalt concrete pavements.

The in-place strength estimation method is based on ultrasonic surface wave measurements. A field test method is proposed, described, and experimentally verified. Verification tests carried out on a range of concrete mixtures with varying aggregate type and cementitious material, all of which satisfy the requirements of "A3" concrete as specified by the Virginia Department of Transportation. Two data analysis procedures are proposed. One procedure predicts flexural strength within 50 psi of actual strength determined by direct strength measurement of beams, although the procedure requires 1-day strength and ultrasonic values to be known. The second procedure is more flexible but provides strength estimates with lower accuracy.

Field tests, which were carried out at two pavement sites in Virginia, are reported for both methods. Finally, a detailed description of the required testing equipment and experimental and analytical procedures for both methods are included in the Appendix. Cost savings from implementing the methods are not obvious, since the methods cannot be used to measure the thickness of most concrete pavements for acceptance and payment. The methods can be used to nondestructively evaluate the modulus of rupture of pavements for analysis purposes, but savings would depend on the nature of the analysis.

FINAL CONTRACT REPORT

DEVELOPMENT OF NONDESTRUCTIVE METHODS FOR MEASUREMENT OF SLAB THICKNESS AND MODULUS OF RUPTURE IN CONCRETE PAVEMENTS

John S. Popovics, Ph.D., P.E.
Assistant Professor of CEE

Alex Gibson, Ph.D.
Graduate Research Assistant

Gonzalo Gallo
Graduate Research Assistant

University of Illinois at Urbana-Champaign

Project Manager
David W. Mokarem, Ph.D., Virginia Transportation Research Council

Contract Research Sponsored by
Virginia Transportation Research Council

Virginia Transportation Research Council
(A Cooperative Organization Sponsored Jointly by the
Virginia Department of Transportation and
the University of Virginia)

Charlottesville, Virginia

December 2005
VTRC 06-CR9

NOTICE

The project that is the subject of this report was done under contract for the Virginia Department of Transportation, Virginia Transportation Research Council. The contents of this report reflect the views of the authors, who are responsible for the facts and the accuracy of the data presented herein. The contents do not necessarily reflect the official views or policies of the Virginia Department of Transportation, the Commonwealth Transportation Board, or the Federal Highway Administration. This report does not constitute a standard, specification, or regulation.

Each contract report is peer reviewed and accepted for publication by Research Council staff with expertise in related technical areas. Final editing and proofreading of the report are performed by the contractor.

ABSTRACT

This report describes work to develop non-destructive testing methods for concrete pavements. Two methods, for pavement thickness and in-place strength estimation, respectively, were developed and evaluated. The thickness estimation method is based on a new hybrid approach that combines frequency domain (impact-echo) and time domain (seismic) data. This new method makes use of a fuller understanding of the dynamic wave phenomenon, which was developed during the course of the work. The effects of material property gradients (due to aggregate segregation and moisture variation) through the slab thickness are compensated for in the method. A field testing method is proposed, described, and experimentally verified. Verification tests carried out on full-scale concrete slabs cast on granular base show that the new method provides more accurate thickness estimates than those obtained by the standard impact-echo procedure. On average, the error between predicted thickness and actual thickness determined by cores is less than 6 mm, although some individual estimates exceed this error value. However, the new method does not work on concrete over asphalt or cement-treated base (which accounts for most concrete pavements) or on full-depth asphalt concrete pavements.

The in-place strength estimation method is based on ultrasonic surface wave measurements. A field test method is proposed, described, and experimentally verified. Verification tests carried out on a range of concrete mixtures with varying aggregate type and cementitious material, all of which satisfy the requirements of "A3" concrete as specified by the Virginia Department of Transportation. Two data analysis procedures are proposed. One procedure predicts flexural strength within 50 psi of actual strength determined by direct strength measurement of beams, although the procedure requires 1-day strength and ultrasonic values to be known. The second procedure is more flexible but provides strength estimates with lower accuracy.

Field tests, which were carried out at two pavement sites in Virginia, are reported for both methods. Finally, a detailed description of the required testing equipment and experimental and analytical procedures for both methods are included in the Appendix. Cost savings from implementing the methods are not obvious, since the methods cannot be used to measure the thickness of most concrete pavements for acceptance and payment. The methods can be used to nondestructively evaluate the modulus of rupture of pavements for analysis purposes, but savings would depend on the nature of the analysis.

FINAL CONTRACT REPORT

DEVELOPMENT OF NONDESTRUCTIVE METHODS FOR MEASUREMENT OF SLAB THICKNESS AND MODULUS OF RUPTURE IN CONCRETE PAVEMENTS

John, S. Popovics, Ph.D., P.E.
Assistant Professor of CEE
University of Illinois at Urbana-Champaign

Alex Gibson, Ph.D.
Graduate Research Assistant
University of Illinois at Urbana-Champaign

Gonzalo Gallo
Graduate Research Assistant
University of Illinois at Urbana-Champaign

INTRODUCTION

For a new portland cement concrete (PCC) pavement to reach its designed service life, it must be designed and built with a proper combination of adequate slab thickness and in-place strength, both of which are selected for the traffic load that the pavement is expected to bear. Therefore, as part of the quality control/assurance (QA/QC) process, it is essential for every newly constructed PCC pavement to be inspected soon after construction is completed (within 28 days) to verify that the contractor has complied with specifications on thickness and strength of the concrete slab. In order to apply an effective QA/QC process the pavement properties (thickness and strength) must be determined with a certain level of accuracy. In a recent study on performance-related specifications, Graveen (2001) recommended that concrete pavement thickness be determined with an accuracy of ±6mm (±1/4 inch) and modulus of rupture with an accuracy of ±345 kPa (±50psi) in order to ensure reasonable and appropriate application of such QC/QA specifications. In fact, the Indiana Department of Transportation now uses those values in its performance-based specifications for concrete pavements (IDOT, 2005).

At present, such verification involves drilling or sawing samples from each newly constructed concrete pavement so that the slab thickness and strength can be measured by prescribed standard methods. Since coring is time-consuming and leaves undesirable discontinuities in a pavement, there is reluctance in carrying out this inspection in a statistically thorough manner. There is, therefore, a need for rapid and nondestructive alternative methods that can be used in place of coring. With such nondestructive evaluation (NDE) methods, the inspection can be conducted at more sampling locations on a pavement for improved pavement quality assurance testing.

Existing NDE Methods for Thickness

To date, no NDE methods have yet been successfully developed to provide reliably the accuracy required for quality assurance of new construction. The standardized Impact-Echo method (ASTM C1383) can provide estimates of pavement thickness under ideal testing conditions. However, the accuracy of the method is lessened by point-to-point variations in P-wave speed (C_p) of the concrete (Clemeña 1994). Additionally, accuracy is compromised to some extent by material property variations throughout the pavement thickness, such as internal moisture content gradients and fresh concrete segregation at the time of placement, and by the nature of the underlying sub-base. Ground-penetrating RADAR (GPR) can provide estimates of pavement thickness also, especially for asphalt pavements. However, the same disturbing influence of varying material composition and, therefore, microwave speed across a project can lead to substantial inaccuracy of the method for concrete pavements (Clemeña and Steele 1988; ACI 1998).

Existing NDE Methods for Strength

No completely non-destructive technique—excluding the so-called semi-destructive tests such as the break off and pull-out tests—is yet available for estimation of in-place concrete strength (ACI 2003). The maturity method, which should be considered a sensing or monitoring method rather than a non-destructive testing technique, has been applied to determine strength development in concrete. Maturity tests are used to estimate the in-place strength development by monitoring the internal temperature over time. The gain of strength of concrete is a result of the exothermic chemical reactions that take place between the cementitious materials and water. The rate of the chemical reactions is related to the internal concrete temperature history. The extent of hydration and the strength gain can therefore be estimated by the internal thermal history of the concrete (ACI 2003). The internal thermal history is used to calculate a maturity index, which is based on pre-established behavior, and correlated to in-place strength. The limitation of this method is that it can only be used to determine the strength development of freshly placed concrete, and the internal temperature must be continuously monitored after placement, for example with embedded sensors. The maturity method has certain variability which depends on the instrumentation being used. The method is based on the assumptions that there is sufficient water for continued hydration and that the concrete in the structure is the same as that used to develop the initial strength-maturity relation. ACI 228 rates this method as very good for strength determination of new concrete, but only if it is verified by other tests. The method is specified by ASTM C1074 (ACI 2003).

The Proposed Approach

The NDE methods proposed here have the potential to provide a higher level of accuracy than other methods previously considered. The methods make use of: (1) a hybrid time-domain/frequency domain measurement that directly determines the pavement thickness without the need for external calibrations or concrete property assumptions; (2) a modified existing frequency domain method for improved pavement thickness measurement; and (3) surface wave velocity and self-compensated transmission measurements to provide more direct correlation to

the in-place strength relevant to concrete pavement, in particular the modulus of rupture (MOR). MOR represents the flexural strength of the concrete, which is a better indicator of concrete quality and performance for pavements than is compressive strength.

PURPOSE AND SCOPE

Toward fulfilling this need, the described proposed investigation aims to achieve the following:

- Develop the basis and testing protocol of NDE for accurate measurement of concrete pavement thickness (with an accuracy of ± 6mm), regardless of surface roughness, base material type and surface condition, surface tining condition, and material internal moisture condition;
- Develop the basis and testing protocol of NDE for determination of in situ flexural strength (with an accuracy of ± 50 psi); and
- Verify the performance of developed testing protocols on actual pavement structures in Virginia.

METHODS

Pavement Thickness Determination

Two different approaches were initially proposed and investigated for the task of nondestructive pavement thickness determination: a time domain method (seismic reflection) and a frequency domain technique (modified impact-echo). Based on the findings from the initial efforts, a third hybrid method (seismic/impact echo) was developed. Each is described in detail in the following.

Design of Experimental Testing Set-up: Seismic Reflection

Basic Concept

The underlying concept of the seismic reflection method is the detection of wave pulse arrivals which arise from reflections off the lower surface of the top layer of a pavement system, at some given horizontal distance (x_i) from the wave source (impact). The travel time of such a signal is directly proportional to the distance, from which thickness can be deduced through geometry. The general testing scheme consists of a wave source and surface-mounted sensors, as illustrated in Figure 1.

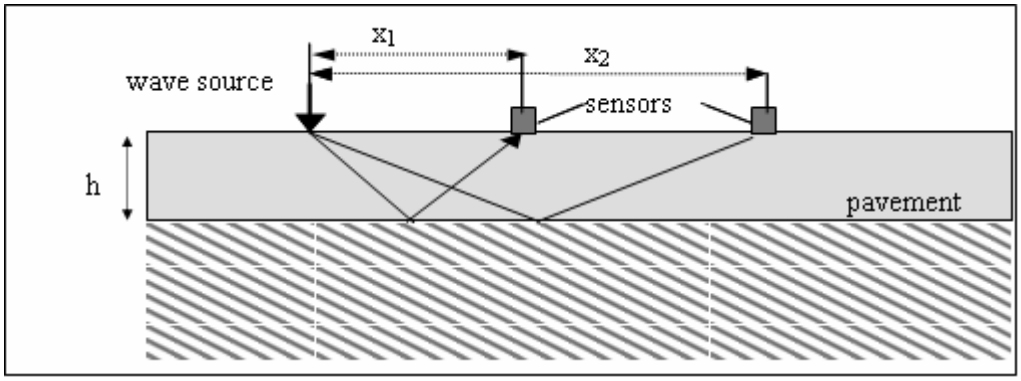

Figure 1: Basic setup illustrating the seismic reflection concept.

Wave energy is partially reflected at an interface between two different materials. Relative amounts of transmitted and reflected energy are a function of the contrast in acoustic impedance between the two materials, thus the amplitude of reflected energy is greater for highly contrasting materials, such as the case of a concrete/air interface.

The reflection set up by an incident wave consists of both initial compression wave (P-wave), shear wave (S-wave), and subsequent mode-converted (both P- and S-wave) components. However, these arrival are only detectable by the surface sensor if they precede the direct surface wave (commonly called the "Rayleigh surface wave" to distinguish it from the preceding direct P-and S-wave rays that propagate along the surface), which has a much higher amplitude and obscures all subsequent arrivals in the signal. Separation between direct and reflected wave arrivals must also be greater than the wavelength of the signal in order for a distinct arrival to be resolved.

Testing Equipment

The source receiver spacing should be sufficiently large to allow the reflected arrivals to precede the direct Rayleigh surface wave, and the generated wave pulse should have appropriately short duration, less than 40 microseconds in order to be resolved in the time domain signal. An additional desired characteristic of the wave excitation source is generation of sufficiently high wave energy needed to propagate the required distance of several meters. Spherical steel impactors have proven to be very effective in producing a broadband propagating pulse through concrete. The maximum frequency of the signal is inversely proportional to the size of the impactor, while the velocity of the ball at impact is directly proportional to the amount of energy it transferred into the system. Therefore an ideal case results from a small steel ball projected at high velocity, but not so high as to cause serious damage to the concrete surface. A good solution was found in the use of a spring-loaded, low muzzle velocity (70 m/s) commercially available BB-gun, shown in Figure 2. The diameter of the spherical steel BB is 4.5 mm.

Further requirements for the impactor unit are accurate targeting ability, consistent input energy, and the capability of triggering a data acquisition system by means of an electrical pulse at the moment of impact. The BB-gun was modified by adding a clear Perspex box at the end of

the barrel, which has the multiple functions of protecting the user against ricochet, regulating the position of the gun for consistency and targeting, and providing support for the laser diode sensors used to provide a trigger signal.

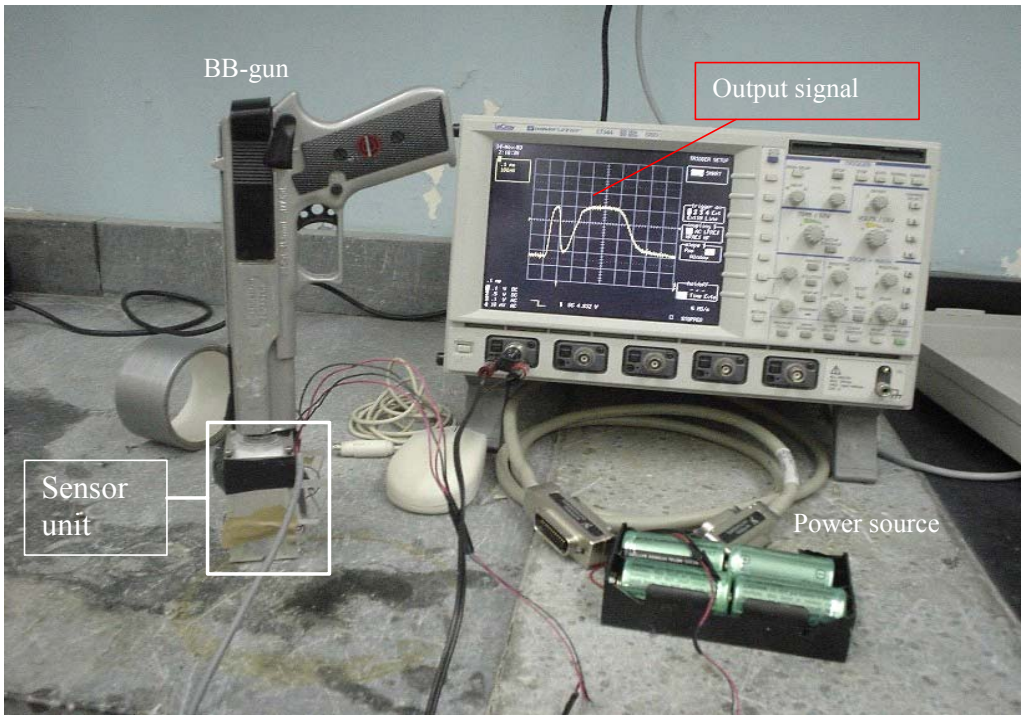

Figure 2: Developed wave source: controlled BB-gun impactor, and nature of trigger signal.

In order to provide a trigger signal relative to the moment of impact, a pair of laser infrared diode sensors was mounted in the casing, level to the surface and positioned so that the trajectory of the fired BB would intersect the beam immediately before striking the surface. The diode circuit is set up so that interruption of the infrared beam is registered as a change in voltage, defined as a trigger event when the instrument is connected to a digital oscilloscope. The level of the beam was raised to approximately 1 mm above the surface; therefore both downward and rebound sections of the BB's passage can be identified. On a smooth steel plate the zero-time of impact could be determined from the diode sensor signal with a level of accuracy of the order of ±2 microseconds. On a rough concrete surface however, the same accuracy fell to the order ±15 microseconds, largely as a consequence of variations in the level of the concrete surface, as the BB traveling at 67 m/s will take 15 microseconds to cover an additional 1 mm, and significant variability in the rebound velocity, which could be related to changing local surface material quality.

The data acquisition system consists of an oscilloscope, signal amplifiers, and miniature accelerometers (PCB Piezotronics model 352B10). These accelerometers were used as wave sensors because they are sensitive (10.89mV/g at 100 Hz), small (1 g mass) and have a broad frequency response (flat response range from 3 to 10000 Hz), which is needed to accurately detect waves generated by an ultra-short duration impact. The sensors are easily mounted on the surface of concrete using a small amount of coupling wax. The digital oscilloscope used in the laboratory testing setup is a LeCroy Waverunner, model LT344. The digital oscilloscope

gathers 10,000 points for each signal at a resolution of 8 bits. A portable computer is used to gather, analyze and store signal data.

Figure 3 shows a sketch of the developed field testing configuration. The method makes use of a series of impacts over a range of source-receiver spacing, lessening the effect of abnormalities and variability in material properties. Two accelerometers are mounted on the pavement surface at .5 m spacing (default value). The sensor spacing can be reduced if needed, although it should not be less than 10cm in order to assure accurate sensor distance measurement. A configuration of impact locations are set at 10 cm intervals along a line away from the sensors. Therefore a pair of signals is obtained at each location that the BB-gun is fired.

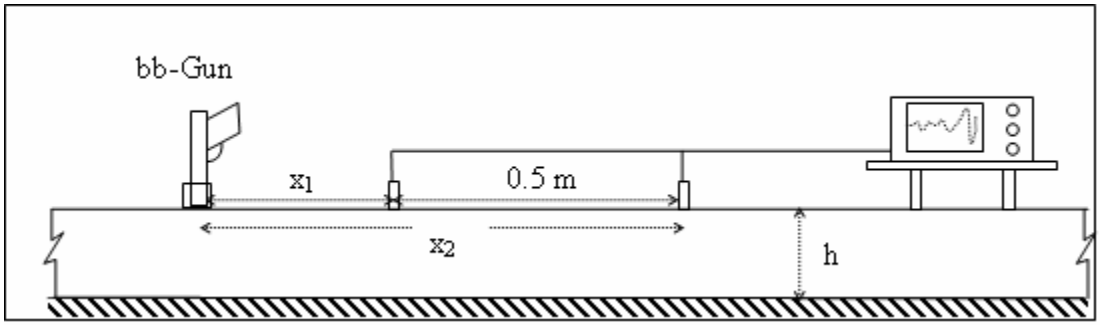

Figure 3: Sketch illustrating the field testing setup.

Analysis Approach: Basic Seismic Reflection

At first, the simply-reflected P-P wave pulses were studied in an attempt to back-calculate pavement thickness. However, results from initial experimental tests demonstrated that the reflected P-P wave pulse is, in fact, not readily observed in the wave signal obtained with the described testing configuration. Rather, other pulse arrivals consistently dominate the dynamic response.

A dynamic finite element model (FEM) was developed to simulate wave propagation in an elastic plate to determine the nature of the wave propagation signals. A point load on a 3-D plate was simulated by means of a 2-D model using quadratic axis-symmetric elements with a nodal impact position at the axis of symmetry. The plate was modeled as having nominally-infinite lateral dimensions and no distributed support along the base. Infinite (energy absorbing) boundaries were set at the outer edge in order to minimize interference from edge reflections. Isotropic, homogeneous, linear-elastic material properties were assumed, valid for low strain and low frequency deformations in concrete. Quadratic elements were used (ABAQUS definition: CAX8) with 5 mm sides and full integration capabilities, giving a maximum resolvable frequency of approximately 100 kHz. The impact force was provided as a semi-$\sin^3$ shaped function of 22 microsecond duration, a close representation of the actual force provided by the BB gun. Nodal acceleration (out-of-plane orientation) histories were recorded along the top surface. Typical computed acceleration responses are presented in the form of a waterfall plot in Figure 4, where theoretical arrivals times for all wave modes are superimposed as lines. The strongest peaks in the measured response correspond to the direct Rayleigh surface wave

arrivals. Of the remaining wave pulses, the most excitable were found to be symmetrical mode-converted reflections, consisting of equal numbers of P-wave and S-wave ray-paths. The first two configurations of this type, the PS and PPSS reflections, are graphically illustrated in Figure 5. The wave front generated by these arrives coincide with local positive maxima in the acceleration signal.

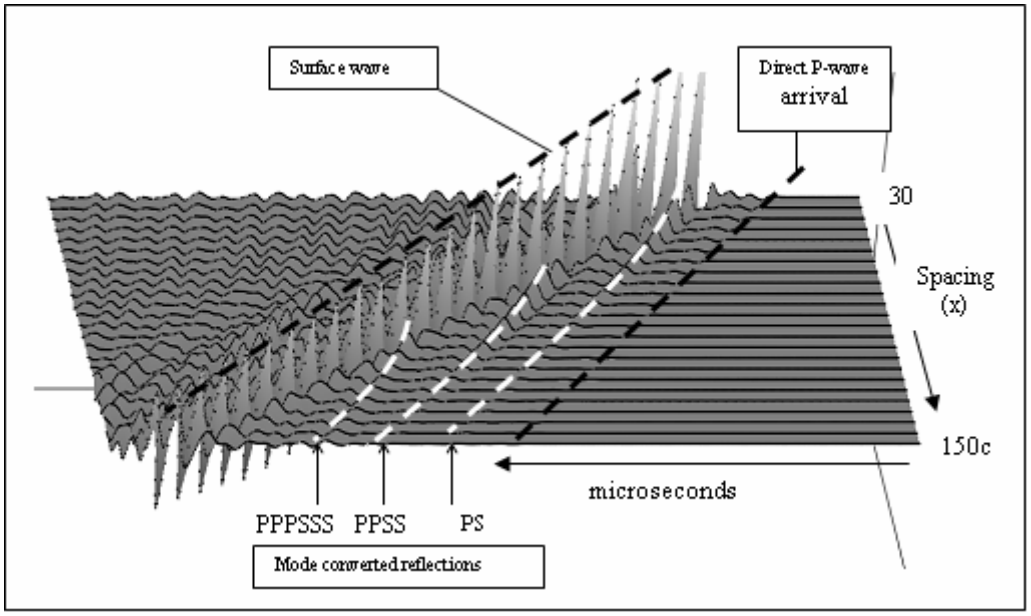

Figure 4: Waterfall plot of FEM out-of-plane acceleration history showing arrival patterns of direct P and R waves and the first three symmetrical mode-converted arrivals.

Thus, the originally proposed approach was modified to make use of these mode-converted wave pulses. Unfortunately, the computation of the arrival time for the mode-converted wave is more complicated than that of the simple P-P reflection, as the P and S waves have different velocities. The arrival time (t_{ps}) in this case can be expressed in terms of a new variable (a) which represents the projection of the reflection point along x

$$t_{ps} = \frac{\sqrt{(ax)^2 + h^2}}{C_P} + \frac{\sqrt{((1-a)x)^2 + h^2}}{C_S}. \qquad (1)$$

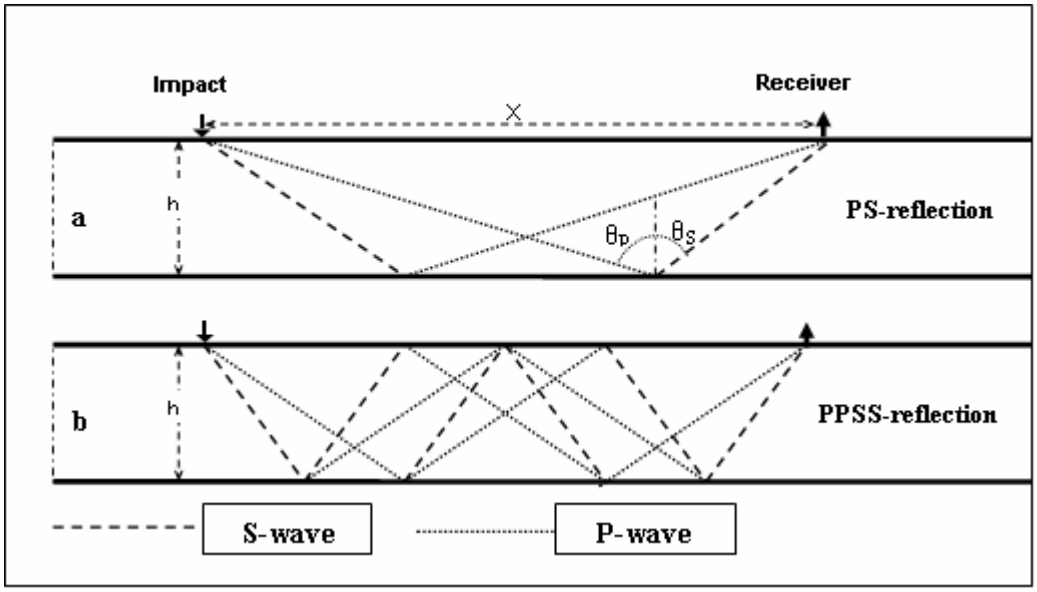

Figure 5: Schematic representation of the first two symmetrical mode-converted arrivals, PS (a) and PPSS (b). Compression wave-paths are represented by dotted lines and shear wave-paths by dashed lines.

A basis for a can be developed starting from Snell's law:

$$\frac{Vp}{Vs} = \frac{Sin(\theta_p)}{Sin(\theta_s)} \tag{2}$$

where θ_p and θ_s are the reflection angles of P- and S-waves respectively.

It is evident that a depends not only on the geometry, but also on material properties, namely Poisson's ratio which defines the ratio between compression and shear velocities. Nevertheless, an accurate relationship between sensor spacing, wave velocity and slab thickness can be obtained by making use of numerical approximation. Based on this approximation, mode-converted PS family pulse arrival times for given configurations of thickness and material properties can be obtained as a function of source receiver spacing. In order to monitor both PS and PPSS arrivals, and also to precede the Rayleigh wave arrival, the ideal wave source to sensor spacing was found to lie between 4 and 8 times the slab thickness

Due to the difficulty in establishing an accurate impact zero-time in the testing setup, however, the approach of interpreting PS and PPSS arrivals directly proved impossible. Because of this limitation no useful results were obtained. However, a new approach was developed where relative arrival times of seismic wave reflections within a single signal could be utilized in conjunction with impact-echo frequency data. This new hybrid approach relies on analysis based on guided wave (Lamb wave) theory, which is described in a subsequent section.

Design of Experimental Testing Set-up: Modified Impact-Echo

Basic Concept

The impact-echo frequency represents the local dynamic resonance response of a structure that is subjected to a light impact event applied to the surface. The out-of-plane surface displacement, with respect to time, is monitored with a sensor at a location near by the impact event. The time-dependent displacement response by itself cannot be interpreted in most cases. However, the signal can be mapped to the frequency domain by applying a Fourier transform. The result of the transformation is complex-valued, so the amplitude of the transform is usually presented at each point, which is now a function of frequency. The amplitude spectra can be interpreted directly wherein the frequency values at signal maxima (peaks) are recorded. In the case of plate-like structures, such as slabs, the fundamental impact-echo frequency (frequency at the lowest-valued significant peak) F is related to the compressional wave velocity of the material C_P and the slab thickness *h*

$$F = \beta C_P / 2h \quad (3)$$

where β is a dimensionless correction parameter (Sansalone 1997, Sansalone and Street 1997). The method is standardized in ASTM C1383, where β is assigned the constant value 0.96 for slab structures.

One cannot obtain the thickness directly from the frequency value alone since h, C_p and β are coupled in the formulation, in Eqn. 3. Previous studies have demonstrated that an estimated, constant value of C_P in Eqn. 3 does not provide the needed thickness accuracy because of localized natural variation of C_P within the concrete along the length of the slab (Clemeña 1995). Thus the ASTM standard procedure specifies a direct measurement of C_P, which is carried out along the top surface of the pavement. The P-wave time of flight between two sensed points is determined by measuring the difference in the time of the first arrival (very first departure from signal baseline value) of the surface-propagating P-wave pulse in each signal; the wave pulse is generated by an impact event applied to the surface at another nearby location. The standard specifies the sensor to be a broad-band piezoelectric transducer that responds to surface displacements; in this report, this type of sensor is called a "displacement transducer." In the case of free slabs, where access to the opposing surfaces is available, another measurement of C_P can be obtained: C_P determined along the path through the thickness of the slab. The standard process to measure the through-thickness ultrasonic pulse P-velocity (UPV) is given in ASTM C597. The P-wave time of flight through the slab thickness is determined by measuring the time required for a P-wave pulse to travel from sending to receiving transducers that are axially aligned at testing points on opposing slab surfaces. Through-thickness C_P is then directly determined knowing the thickness of the slab.

In order to obtain accurate thickness measurements with the impact-echo method, accurate and reliable values of C_P and β must be used in Eqn. 3. To date the standardized impact-echo method does not provided the needed accuracy for pavement thickness. Thus the effort in this section will be to improve the accuracy of impact-echo method by modifying the method with regard to improved values of C_P and β.

Testing Equipment

The impact-echo tests were carried out using a commercially-purchased impact-echo testing package that satisfies the requirements set out in ASTM C1383. This equipment package consists of a Windows 98 laptop computer containing the testing software, a set of spherical steel impactors, and two sensing transducers (displacement transducers) separated a fixed distance by a spacing bar. The Impact-Echo software, developed by Impact-Echo Instruments, LLC guided the data collection, analysis (FFT) and storage processes. The P-wave signal data were digitized using 2048 data points with 0.5μs sample interval. In each signal the P-wave arrival time was determined by the controlling software.

The impact-echo resonances were excited using a 12 mm diameter impactor. As per ASTM C 1383 requirements, the source-transducer spacing did not exceed 40% of the known thickness of the slab. Three repeated measurements were performed at each point, and the average value was reported. The systematic error of the testing configuration is that caused by signal digitization and processing limitations (Sansalone and Street 1997). The total systematic error can be computed assuming nominal values of Cp (e.g., 4000 m/s) and h (e.g., 180 mm). Following (Sansalone and Street 1997), velocity error $e_p = \pm 0.0067$, frequency error $e_f = \pm 0.023$, and total error $e_t = \pm 0.024$. This gives a theoretical systematic thickness error of ± 4.3mm in this case, which is within the desired accuracy target.

The UPV tests were carried out using commercially purchased UPV testing unit that satisfies the requirements set out in ASTM C597. This equipment package consists of a pair of 54 kHz ultrasonic transducers and an associated timing and display unit. The unit measures the P-wave time of flight and displays the result to the nearest 0.1 μs.

Experimental Specimens

Three plain concrete (without steel reinforcement) test slabs were cast. The slabs have the same nominal thickness (18 cm), with natural variation and error as the only reasons for differences in actual thickness at a given location. This practice simulates actual practice, where a target nominal thickness is sought by the paving contractor. The slabs differ in concrete composition, however, to simulate the range of concrete classes used in pavements. The slabs are tested in the days after casting, again simulating tests on new concrete pavements for quality-based specification compliance. The tests were carried out over several weeks, to determine any effect due to the material property changes owing to hydration in these first few weeks after casting.

The slabs were cast horizontally into pre-formed wooden forms, including the bottom surface. The cast concrete slab forms measured 152cm x 152 cm x 18 cm (60 inches x 60 inches x 7 inches). The fresh concrete was spread and compacted by hand, and the top surface struck off. The slabs' top surfaces were kept moist and covered with an impermeable sheet for 24 hours. Approximately one day after casting, the slabs were de-molded and testing locations were identified and marked on each surface of the slab. Each slab has a different concrete mixture,

simulating a range of concrete strengths: normal strength (slab 1), moderate strength (slab 2) and high strength (slab 3). Three companion cylinders (150mm x 300mm) were also cast for each slab and the dynamic Young's modulus (ASTM C 215) and through-thickness ultrasonic pulse velocity (ASTM C597) of those cylinders were determined at the age of 28 days after mixing. All concrete was obtained from a local ready-mix supplier. The coarse aggregate was crushed limestone with a maximum size of 19 mm. The fresh concrete had slump of 75 mm ± 10 mm. All concrete mixtures contained entrained air, with total air content of 6% ± 1%.

For each slab, two different testing locations were identified. Impact-echo (one-sided velocity and resonance test components) and through-thickness ultrasonic pulse P-velocity (UPV) tests were carried out at those defined points. The tests were repeated over the course of several weeks at the same testing locations. Then full-thickness cylindrical core samples were taken at those same testing locations, upon which the actual slab thickness was determined directly. Subsequent tests were then carried out on the core samples.

At the conclusion of the NDE tests, two cylindrical core samples were drawn from the concrete slabs at the identified testing locations. The slabs were cored using a 3.75 inch diameter wet power coring machine. The actual thickness of the slab at the testing locations were then determined directly from the core sample using a set of calipers. Subsequently, the cores were sawn into 5 disks, each disk having a thickness of approximately 40 mm. The disks were then subjected to UPV measurements through the 40 mm thickness of the disk.

Analysis Approach: Guided Wave Model

Due to the uncertainty in the physical significance and appropriate value for β, a analytical study on this topic was carried out. The basis of this approach is again guided wave (Lamb wave) theory. The use of guided wave theory has precedents in the prediction of impact-echo frequencies in structures with solid and hollow circular cross-sections (Popovics 1997), as well as in air-coupled frequency measurement in resonating plates (Holland and Chimenti 2003). In the latter case plates were found to present a strong resonance at the zero group velocity frequency of the first-order symmetric (S_1) Lamb mode. Group velocity (C_G) of a given mode represents the speed of in-plane energy propagation along the length of the plate. Thus the C_G=0 frequency represents a stationary wave motion condition (Achenbach 1973) where energy does not propagate away, which would in effect be measured as a resonance by a fixed sensor.

Consider the two geometrically simplest resonance cases: one composed purely of compressive action (P-wave) and the other of pure shear (S-wave) action. In both of these configurations the upper and lower surfaces must remain parallel to conserve the respective pure compressive and shear actions implied by infinite wavelength, or by definition, a wavenumber (k) of zero. These modes are directly related to shear and compression properties of the material, frequencies are related to return-journey of the compressive and shear waves respectively. The former corresponds to Eqn.3 where β = 1. In fact this was the assumed impact-echo equation initially when the method was first developed. Later, β was modified to be 0.96 in order to match experimental observations.

Now consider guided Lamb waves. Lamb waves, also known as guided plate waves, are propagating resonances which occur in free plates (Achenbach 1973). They are formed by coupled longitudinal and transverse wave motion, that is to say the interaction of P and S waves, and include an infinite number of individual symmetrical (S) and anti-symmetric (A) solution modes. Each lamb mode has a distinct phase velocity, which unlike the body and surface waves, is dispersive (i.e. is a function of frequency). Lamb-wave solutions (dispersion relationships) are obtained from the roots of the corresponding Rayleigh-Lamb equations; the S Lamb (Equation 4) modes and A modes (Equation 5) can be expressed in terms of normalized frequency (Ω) and normalized wave-number (ξ) (Achenbach 1973)

$$0 = \frac{\tan(\sqrt{\Omega^2 - \xi^2} \cdot \pi/2)}{\tan(\sqrt{\Omega^2/\kappa^2 - \xi^2} \cdot \pi/2)} + \frac{4\xi^2 \sqrt{\Omega^2/\kappa^2 - \xi^2}\sqrt{\Omega^2 - \xi^2}}{(\Omega^2 - 2\xi^2)^2}, \tag{4}$$

$$0 = \frac{\tan(\sqrt{\Omega^2 - \xi^2} \cdot \pi/2)}{\tan(\sqrt{\Omega^2/\kappa^2 - \xi^2} \cdot \pi/2)} + \frac{(\Omega^2 - 2\xi^2)^2}{4\xi^2 \sqrt{\Omega^2/\kappa^2 - \xi^2}\sqrt{\Omega^2 - \xi^2}}, \tag{5}$$

where $\Omega = \frac{2hF}{C_S}$ and $\xi = \frac{hk}{\pi}$, h is the full plate thickness, F is frequency and C_S is the transverse (shear) wave velocity. Dispersion curves defined in Ω vs. ξ space by individual solutions of the Rayleigh-Lamb equation must be traced by means an appropriate root-finding algorithm, since there is no analytical solution to the equations. The frequency-dependent (dispersive) phase velocity (C) of each of these modes may be obtained from the normalized parameters Ω and ξ and specific model parameters (h and C_S)

$$C = \frac{2\pi F}{k}. \tag{6}$$

The normalized wavenumber vs. frequency dispersion curves obtained from the Rayleigh-Lamb equations for a specific value of Poisson's ratio (ν=0.2) are shown in Figure 6. We note that for the two fundamental modes, A0 and S0, group and phase velocities converge towards the theoretical Rayleigh wave velocity as frequency increases. S1 and A1 modes group velocities (slope of the curve) drop towards zero values at specific frequencies, indicating stationary resonances at these frequencies

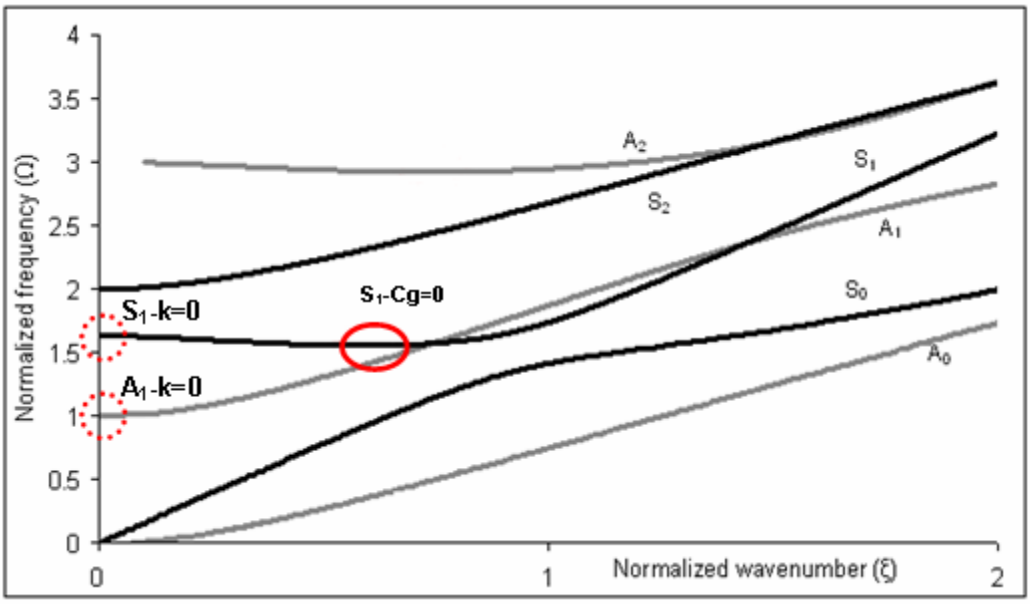

Figure 6: Dispersion curves for the first three symmetrical and anti-symmetrical Lamb wave modes, illustrating zero-group-velocity conditions at frequency minima (solid circle) on the S_1 curve (ν=0.2), and zero-wavenumber frequencies (dotted circles) for S_1 and A_1 modes.

The two pure shear and compressional (zero wavenumber) resonance frequencies described above correspond to the normalized frequency values at the intersection of the A_1 and S_1 curves with the vertical axis, indicated with dotted circles in Figure 6. Also highlighted is the section of the S_1 curve where frequency reaches a local minimum, which is by definition the zero group velocity frequency. The shape of the S_1 curve on Figure 6 indicates that resonance will not occur at the k=0 condition, as the Ω vs. ξ slope is negative indicating a negative group velocity. A slightly lower frequency, corresponding to the (C_G=0) condition will be the actual resonance frequency, accounting for the Impact-Echo correction factor β below 1.

The analytical procedure to find exact solutions for β consisted of obtaining the S_1 mode dispersion curve over a range of ν values, by tracing the appropriate roots of the symmetric Rayleigh-Lamb equation; more detail on the computation can be found in (Gibson 2005) and (Gibson and Popovics 2005). The equation must be solved via computational root-searching algorithms as there is no analytical solution.

In order to explore the prevalence of particular frequency components of a given mode in the overall response, we introduce the concept of excitability. The amplitude of each Lamb mode in the plate is proportional the amplitude provided by the excitation force, where the frequency-dependant constant of proportionality is represented by an excitability function. Large excitability values would imply large generated wave amplitude for a given input excitation, and the corresponding frequencies would be more readily measured experimentally. Axisymmetric, 3-D, out-of-plane excitability for symmetric and antisymmetric Lamb modes generated by a point source can be obtained by considering solutions for Lamb wave displacements, solved using a spatial Hankel transform (Ditri et al. 1994). More detail on the nature and derivation of the excitability functions can be found in (Gibson 2005).

Figure 7 shows group velocity plotted against frequency for the first 3 symmetrical and antisymmetrical Lamb modes calculated for a specific set of material properties (h=0.15m, ν=0.2, C_P = 4303 m/s). The fundamental modes (S_0 and A_0) represent high-energy propagating surface modes; the group velocity does not approach zero at non-zero frequency values, implying they cannot construct a (C_G=0) resonance condition.

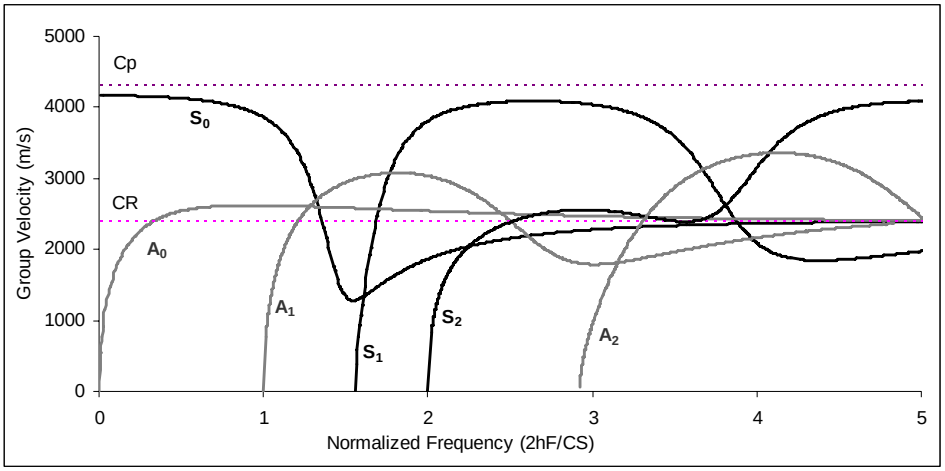

Figure 7: Group velocities of the first 3 A (grey) and S (black) modes calculated for ν=0.2.

In Figure 7 the S_1 mode shows zero group velocity normalized frequency of 1.57, where the curve intersects the horizontal axis. Absolute values of the excitability functions evaluated for the same model parameters are shown on a logarithmic scale in Figure 8. The excitability coefficient for the S_1 is seen to increase dramatically as (C_G=0) frequency (Ω=1.57) is approached, implying a highly-excitable condition. Other significant excitability functions include the A_1 mode, which shows a peak close to the S_1(C_G=0) frequency, but drops to zero at the A_1(C_G=0) frequency where its own resonance condition would be. A second pair of matching peaks, for the A_2 and S_2 modes, are observed at Ω=3.16, corresponding to a low but non-zero A_2 group velocity.

Commercially available Finite-Element Model (FEM) software (Abaqus standard v6.2-7) was used to simulate the transient behavior and resonance frequencies of a plate-like element. In order to simulate a 3-D plate structure with sufficient mesh refinement and within the available computational capacity, a 2-D model was developed using quadratic axis-symmetric elements. In order to simulate a point load on a 3-D plate the impact position was located on the axis of symmetry. The plate was modeled as having nominally infinite lateral dimensions and no support. Infinite (energy absorbing) boundaries were set at the outer edge in order to simulate a plate free of interference from edge reflections. Material properties were assumed homogeneous and linear-elastic, valid for low strain, low frequency deformations in concrete. The size of elements and the lateral dimension of the model (L) were determined via a convergence analysis (Gibson and Popovics, 2005).

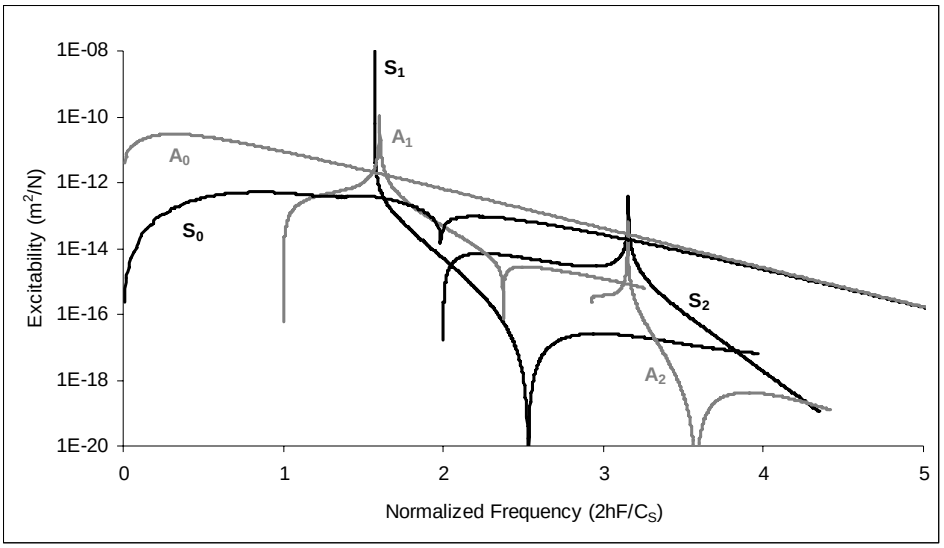

Figure 8: Out-of plane excitability functions for the first 3 A (grey) and S (black) modes calculated for ν=0.2, showing maximum excitability at S_1 (C_G=0).

It has been proposed that the numerical model presents a symmetrical mode with resonance frequency that converges to the theoretical S_1-C_G0 frequency as the number of elements and size of model increase. In order to verify the excitability of this particular mode due to a mechanical impact, a direct time-step integration was carried out on model F5 using a 42 μs $(\sin/2)^3$ impact and 5000 2-μs time-steps. The results show a single well defined peak which coincides, within resolution limits, with the S_1-C_G0 frequency calculated analytically for the same model parameters.

In addition to the verifying convergence, the Finite Element Analysis was validated using experimental data. For this two concrete slabs were tested, with differing material properties. The dimensions of the specimens were such that they could be defined as slabs for impact-echo purposes, with thickness to width ratios smaller than 1:5 (Sansalone and Street 1997). The first specimen consisted of a 18 cm deep rectangular slab with lateral dimensions of 2x2 m, while the second consisted of a 52 cm thick wall with over 3 m lateral clearance in all directions. A laser Doppler vibrometer (Polytec PDV-100) was used to measure the transient out-of-plane velocity response on the physical specimens. This instrument has a frequency range of 0-22 kHz and velocity ranges between ±20 and ±500 mm/s, and requires no surface preparation when used on a flat concrete surface. The impact forces were approximated via a $(\sin/2)^3$ forcing function in the FEM model. The models were run using direct time-step integration using a total of 5000 time-steps, with 10 μs steps for model V1 and 2 μs steps for model V2. Due to physical constraints caused by the equipment, the response was measured at a point 10 cm from the impact. A consistent time-domain configuration was used for the experimental data collection.

A typical out-of plane velocity response from experimental and FEM results over the initial cycles in the time domain is shown in Figure 9 (left). By means of an FFT analysis these responses were converted to frequency domain; the amplitude spectrum is presented in Figure 9 (right). Experimental and FEM plots are found to match adequately in both time and frequency domains, which supports the validity of the FEM model and the initial assumptions.

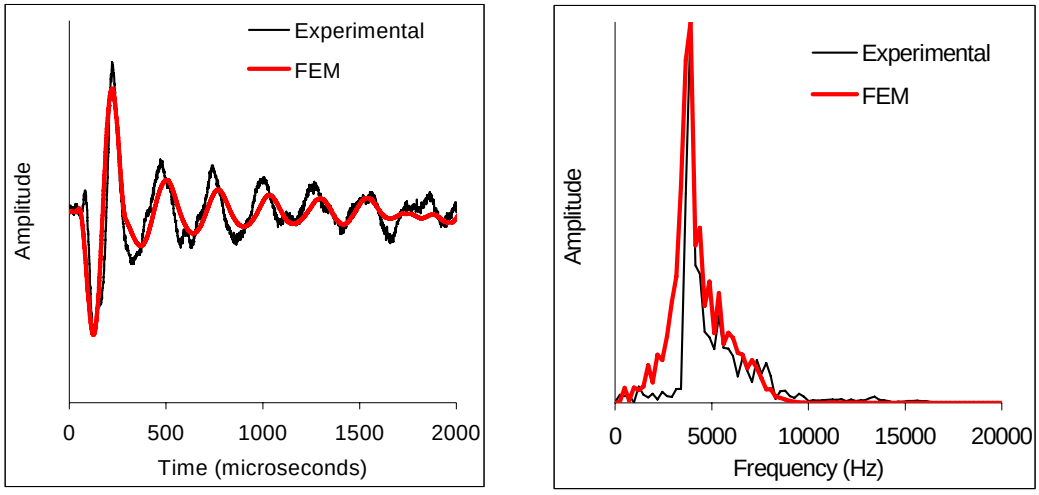

Figure 9: Experimental and FEM (left) time-domain and (right) frequency domain (FFT) transient out-of-plane velocity response at 10 cm from the impact – V2 specimen.

Based on this interpretation, exact theoretical values of β for plate-like structures were computed. These range in value from 0.945 to 0.957 over the normal range of concrete material properties. The dependence of β on Poisson's ratio is thereby illustrated. Such an interpretation, explicitly implying a resonance condition in the plate, accounts for the correction factor of approximately 0.96 which is specified by ASTM standards. For practical purposes, the resulting ν vs. β relationship may be approximated by the second-order approximation, with equation

$$\beta = -0.645\nu^2 + 0.135\nu + 0.952\,. \tag{7}$$

The analytical and FEM data presented so far are representative of a free slab with no underlying support. This is relevant to many practical situations where NDE is often required, as in a free-standing wall or an elevated floor with exposed surfaces commonly found in parking garage structures. In other cases, notably in highway pavements, the slab is supported by a base material that is usually of lower stiffness than concrete. It is important to establish the behavior of such a mode in the case of a slab resting on a different material. This is presented next assuming the Impact-Echo resonance frequency is defined by the zero group velocity frequency of the S_1 Lamb mode.

Lamb wave dispersion as defined by the Rayleigh-Lamb equation is only valid for the case of an infinite plate in vacuum. In the case of a multi-layered system, wave propagation may be predicted by P and S-wave superposition, given the correct set of boundary conditions at each interface. The analytical solution for the case of a multi-layered system was first presented by in 1953, and many publications devoted to such so-called matrix techniques exist in the literature (Ewing *et al.* 1957). Applying the global matrix method, each layer interface is represented with a layer Matrix [D], defined by the layer elastic properties and thickness as outlined below. The individual layer matrices are assembled into a system matrix [S] which ensures all boundary conditions are satisfied simultaneously. The dispersion curves of the

layered system are defined by frequency ($\omega=2\pi F$) and wavenumber (k) combinations which result in a singular [S] matrix (i.e. $|[S]|=0$). More detail on the analytical and numerical aspects of this computation can be found in the thesis written by Gibson (Gibson 2005).

As the objective of this study is to quantify the effects of increasing base impedance, the following analytical step was implemented to provide a non-zero velocity and density in the underlying half-space: base impedance was increased in small steps, and each time a set of solutions for k_i and ω were found along the pre-determined range of k_r values. Solutions were fed through the system in order to provide good initial guesses of k_i and ω at each subsequent step. Solutions were verified using the commercially available software Disperse©, available under license from Imperial College, London. The global matrix solution was implemented over a range of concrete to base acoustic impedance contrasts, by setting a range of base densities between 1600 and 2400 kg/m^3, and C_P values between 10 and 1000 m/s. The original concrete plate properties of C_P=4303.3 m/s, ρ=2400 kg/m^3 were maintained constant. For each case the frequency corresponding to minimum positive group velocity, within the region of numerical stability, was identified as the resonance frequency. The observed variations with respect to the free plate resonance frequency are plotted against half-space/plate acoustic impedance ($Z= \rho C_P$) contrast in Figure 10.

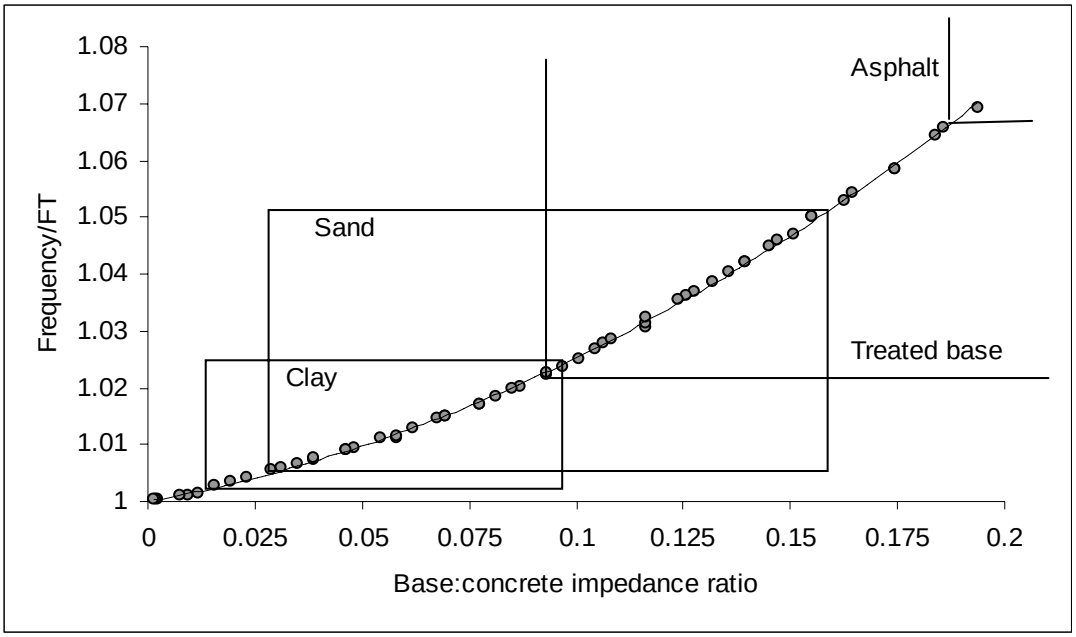

Figure 10: The merged relationship between concrete-base acoustic impedance contrast ratio and the shift in resonance frequency with respect to free plate frequency. A second-order polynomial best fit to the data is shown as a line. Ranges in impedance contrasts for typical base materials are indicated.

The results from a range of different combinations of base properties in Figure 10 appear to follow a consistent relationship, which for the purposes of practical implementation can be approximated by the second-order polynomial

$$\beta_2 = 1.165\left(\frac{Z_B}{Z_C}\right)^2 + 0.137\left(\frac{Z_B}{Z_C}\right) + 1 \qquad (8)$$

where Z_C and Z_B are the acoustic impedance (ρC_P) of the concrete and base respectively, and $\beta 2$ represents a correction factor ($Ft_{(base)}/Ft_{(free)}$).

Variations in impact-echo frequencies owing to base stiffness changes were investigated by experiment. An existing 18 cm thick, 2-by-2 m concrete slab was placed on a freshly poured lean mortar mix serving as a mock-up of a rigid cement-treated base. Prior to setting up the base, eight locations on the slab surface that gave clear and consistent resonances were selected, and Impact-Echo frequencies were measured in the freely-supported state. A mortar mix consisting of a 6:1 mass proportion of sand to Type I Portland cement mix, and sufficient water to provide adequate consistency, was provided as the base. The fresh mortar was placed in a wooden frame to a depth of 75 mm, and leveled prior to lowering the concrete slab onto it (Figure 11). A sample of the mortar was cast separately in an open-ended 20 cm test cylinder to monitor setting via UPV measurement.

Impact-Echo frequency and UPV measurements were taken at several time increments, between 1 to 48 hours after the mortar was mixed. In order to optimize frequency resolution, signal acquisition setup consisted of 5 μs timesteps and 2048 sampling points, and zero-padding was applied to extend the signal duration to 2^{15} points prior to applying the FFT. At each location the impact was repeated five times and averaged in the frequency domain, without normalizing the amplitudes.

The observed differences in frequency spectra at a given location at 1 and 48 hours are presented in Figures 12a and 12b. The shape of the dominant peak in Figure 12b is clearly smaller and broader, confirming the effect of leakage attenuation when the slab is in contact with a more rigid base material. Although it appears significant in the figure, this effect would not be apparent if the spectra were normalized, as is standard procedure with impact-echo data analysis. The peak frequency was found to undergo a small but regular upward shift with increasing base stiffness, also consistent with the theoretical results. A third effect apparent in all the signals is the attenuation, with increasing base stiffness, of low-frequency resonances. These components are apparent between 1 and 5 kHz in Figure 12a, and are attributed to flexural modes and edge effects. The relative amplitude of these modes may be used as a basis for determining the integrity of underlying layers of a pavement slab (Sansalone and Street 1997).

Figure 11: Transfer of the test slab onto the fresh mortar base in preparation for testing.

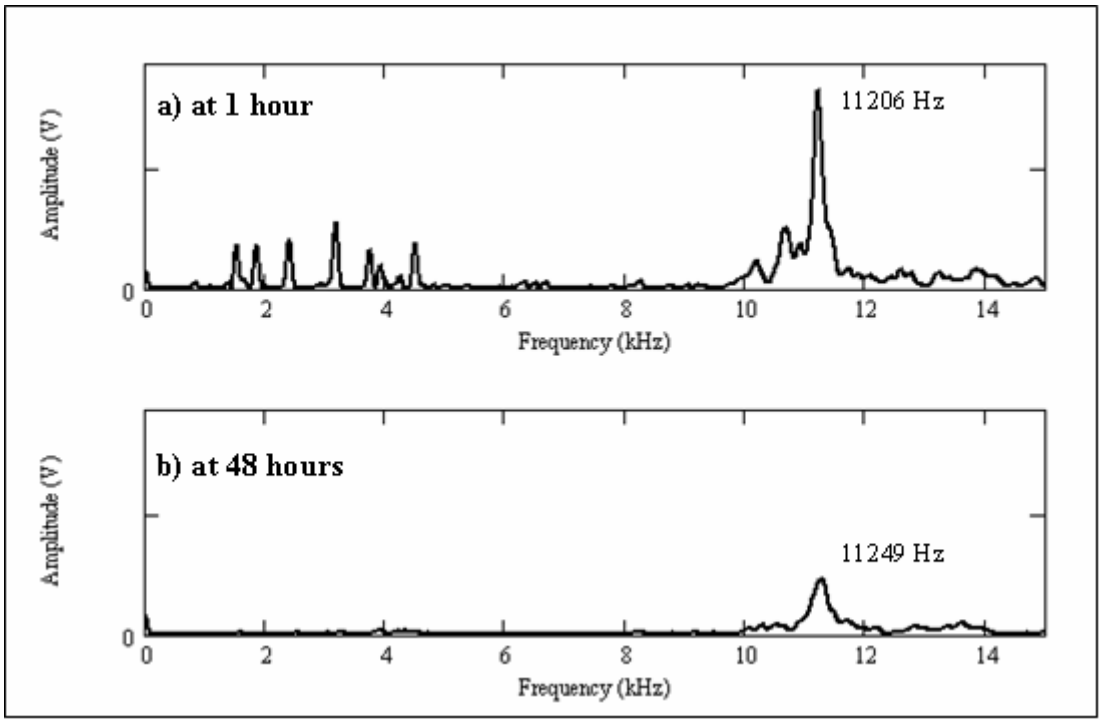

Figure 12: Experimental frequency spectra at a fixed point on the slab at 1 hour (a) and 48 hours (b) after the base mortar mixing.

Ultrasonic pulse velocity (UPV) measurements were taken on the control cylinder from the time the mortar paste solidified, starting at 8 hours. Development of measured UPV indicate a proportionality between C_P (and acoustic impedance) of the base and average frequency shift. These trends are consistent with the predicted theoretical shifts calculated above. The magnitude of the shift, however, cannot be accurately quantified without a more detailed characterization of the bond between the slab and base, assumed to be perfectly tied in the case of the theoretical model. In practice bond quality will vary widely according to material properties and construction methods, and is likely to have a significant effect on theoretical frequency shifts.

As an additional study, the excitability of additional symmetrical and anti-symmetrical modes was also investigated using similar analytical, numerical and experimental techniques similar to those described above. The presence of additional measurable resonances would have potential to improve the accuracy of non-destructive field methods, by providing a basis to determine assumed material properties such as Poisson's ratio and/or base impedance. According to the Lamb wave interpretation for Impact-Echo, resonance frequencies are set up by stationary energy, which corresponds to the zero group velocity condition. This condition is satisfied where the slope of the frequency vs. wavenumber curve is zero, as illustrated in Figure 13.

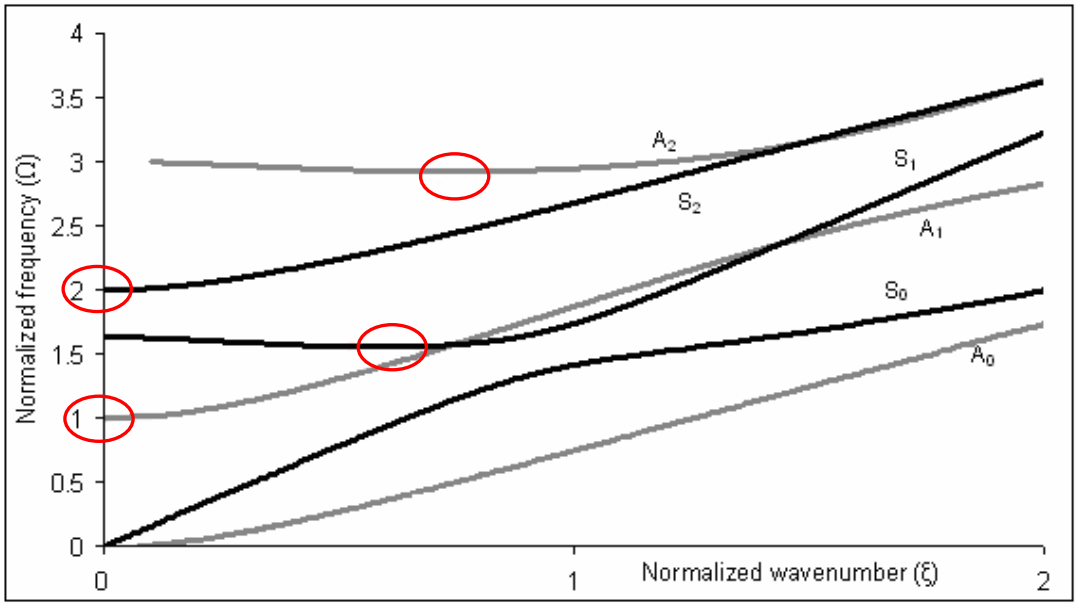

Figure 13: Dispersion behavior of the first three symmetrical and anti-symmetrical Lamb wave modes. Zero-group-velocity conditions on the S_1, S_2 A_1 and A_2 curves indicated by ovals (ν=0.2).

FEM results demonstrate that the natural frequencies associated with the S_1 and A_2 mode shapes, converge to the analytically determined C_G=0 frequencies. Figure 14 shows the frequency spectrum obtained from combined in-plane and out-of-plane acceleration response at 5 cm from the impact on the FEM model. The spectrum shows a pair of peaks that coincide with S_1 (impact-echo) and A_2 zero group velocity frequencies.

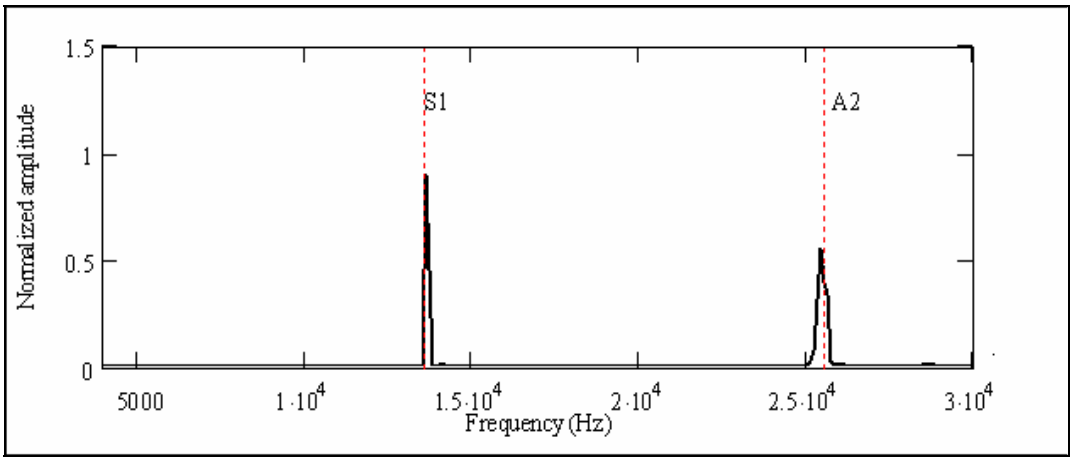

Figure 14: Sum of the spectra of in-plane and out-of-plane acceleration components for the direct time-step integration FEM model, at an impact-receiver spacing of 5 cm. The markers indicate theoretical (C_G=0) frequencies for the S_1 and A_2 Lamb modes.

A possible application of recording both S_1 and A_2 resonance frequencies would be to more accurately characterize material properties. It was observed that while the two frequencies can be normalized with respect to the same parameters, they respond differently to variations in Poisson's ratio. Therefore, for a freely supported slab, the ratio between the two frequencies bears a unique relationship to ν that is independent of thickness and pulse velocity. The relationship can be approximated by a second-order polynomial using the equation:

$$\nu = -3.1476 \cdot \left(\frac{F_{A2}}{F_{S1}} \right)^2 + 10.845 \cdot \frac{F_{A2}}{F_{S1}} - 9.0663 \qquad (9)$$

where F_{A2} and F_{S1} are the A_2 and S_1 resonance frequencies. The excitability of the A_2 mode was verified by measuring the out-of plane acceleration response to an impact of a freely supported slab. Using the obtained frequency peaks (F_{S1} = 8789.1 Hz and F_{A2} =16602 Hz) and the theoretically inferred relationship given in equation 9, a value of 0.188 is obtained, which is within the expected range for concrete.

The impact-echo method, as applied to slabs, is defined to hold while the aspect ratio (width/thickness) does not fall below 5. The structure is defined as having rectangular cross-section for aspect ratios below this value, for which additional resonance frequencies are present in the response (Sansalone and Streett 1997). The effect of nearby boundaries on the accuracy of the Lamb wave resonance based approach is investigated using numerical analysis in this section. Two FEM models were used: a finite axis-symmetrical model for a cylindrical slab, and a plane-strain model representing an infinitely long rectangular section. In both cases 5 mm quadratic elements were used, and as before, the Lanczos eigenmode solver was implemented to obtain the natural frequency associated with the S_1 mode shape. Lateral boundaries were introduced by progressively eliminating elements at the end of the model, effectively reducing the dimensions every consecutive run. Resulting shifts in the S_1 resonance frequency, expressed as a ratio to the infinite plate frequency, were observed. The results show less than 1% variation in resonance frequency for aspect ratios greater than 5:1, confirming the validity of established

impact-echo guidelines. As the plate dimensions approach those of a rectangular beam section (i.e. 5:1 aspect ratio) not only do the fundamental resonance frequencies shift more abruptly, but additional cross-sectional vibration mode resonances appear.

Design of Experimental Testing Set-up: Hybrid Method

Basic Concept

Since the impact-echo phenomenon is modeled well by guided wave theory, it is conceivable that the wave phenomenon associated with the seismic approach is also well modeled by guided wave theory. An effort to model both methods with guided wave theory, then to unify both tests under one fundamental modeling basis would allow for effective combination of the two methods in a hybrid approach. The application of data from two methods allows the elimination of experimental unknowns, such as material wave velocity, Poisson's ratio, etc., in the thickness estimation computation, thereby likely improving performance and accuracy.

Testing Equipment

The same testing equipment, which is described in the seismic and modified impact-echo approaches, is applied for the hybrid test.

Experimental Specimens

Three full-scale (3 m x 4 m plan) concrete slabs were cast atop loosely compacted sand base, with nominal design thicknesses of 20, 25 and 30 cm, denominated S20, S25 and S30 respectively. The concrete mix was based on Virginia DOT highway pavement specifications, with a design 28-day compressive strength of 20.7 MPa (3000 psi) and maximum water-to-cement ratio of 0.49. On-site tests confirmed 6% entrainment air content and a 3 inch slump for the fresh concrete, and test cylinders yielded an average compressive strength of 29.1 MPa (4225 psi) at 28 days. Adequate curing was ensured by covering the slabs with a nylon sheet and maintaining abundant moisture on the concrete surface for the first 8 days. Following the removal of the sheets the surface of the slabs were exposed to hot, mostly sunny conditions typical of central Illinois summer, with average high temperatures of 85° F (24° C).

Analysis Approach: Guided Wave Model

Although the direct arrival times of PS and PPSS wave reflections could not be determined because of experimental triggering limitations, the relative arrival times t_{ps} and t_{ppss} at two accelerometer positions (x_1 and x_2), can be inverted by means of a model which incorporates the rather complex solutions to the Lamb-wave dispersion and ray-path theory and the impact-echo frequency of the pavement section. The model relies on the simultaneous iterative evaluation of thickness and Poisson's ratio to minimize errors between experimental and model data. The normalized Lamb-wave phase velocity dispersion curve is unique for a given Poisson's ratio (ν). A normalized theoretical S_1 dispersion can be imported from a database once a value of ν has been defined. An example set of S1 Lamb wave dispersion curves for a range of Poisson's ratio values is shown in Figure 15.

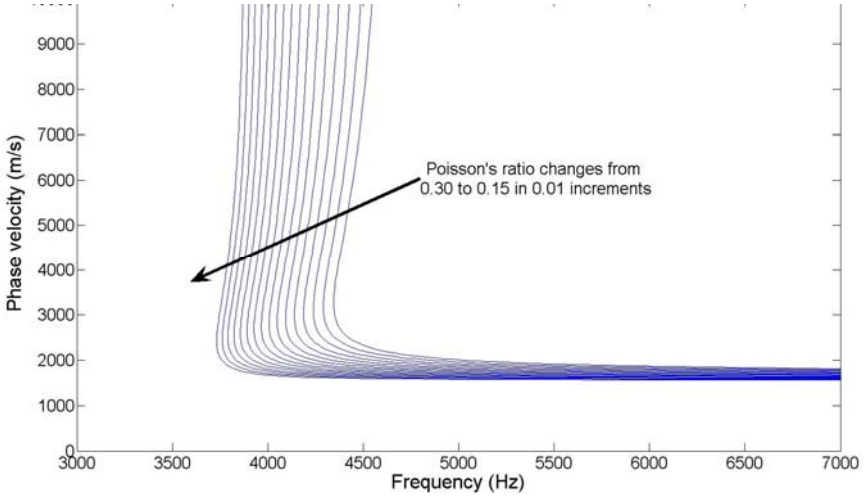

Figure 15: S1 Lamb wave dispersion curves for Poisson's ratio ranging from 0.15 to 0.30 in increments of 0.01. Assumed Cs=1000m/s and h=200mm.

The unknown thickness and Poisson's ratio are obtained by fitting experimental frequency and phase velocity data points, as defined by equations 10 and 11 and a limiting impact-echo frequency value. The normalized dispersion curves are defined by the Rayleigh-Lamb equation. Experimental frequency and phase velocity points are calculated from PS and PPSS arrivals at sensor locations A (near) and B (far), which are separated by a known distance (default value = 0.5 m.)

$$F = \frac{1}{t_{ppss}(B) - t_{ps}(B)}, \tag{10}$$

$$C_{ph} = \frac{0.5m}{t_{ps}(B) - t_{ps}(A)}. \tag{11}$$

A typical dynamic out-of-plane acceleration response is presented in Figure 16, where the direct P-wave arrival is identified as the initial discontinuity of the signal and the surface wave arrival as the zero-crossing prior to Rayleigh-wave peak of significantly higher amplitude. PS and PPSS arrivals can also be identified as the dominant intermediate peaks.

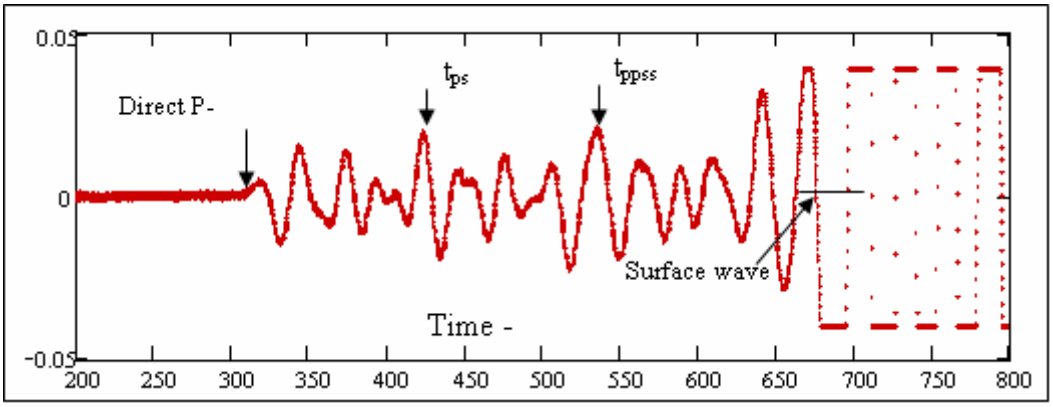

Figure 16: Typical acceleration trace indicating the different wave arrival times.

If a value of concrete C_s is assumed, the value of thickness and Poisson's ratio in the model can be iteratively adjusted in order to obtain a best fit of experimental data (seismic reflection points and impact-echo line) onto the theoretical phase velocity dispersion curve. A set of typical experimental phase-velocity dispersion results is presented in Figure 17. Mean thickness over the testing length is obtained from minimizing squared error between the theoretical and experimental dispersion curves.

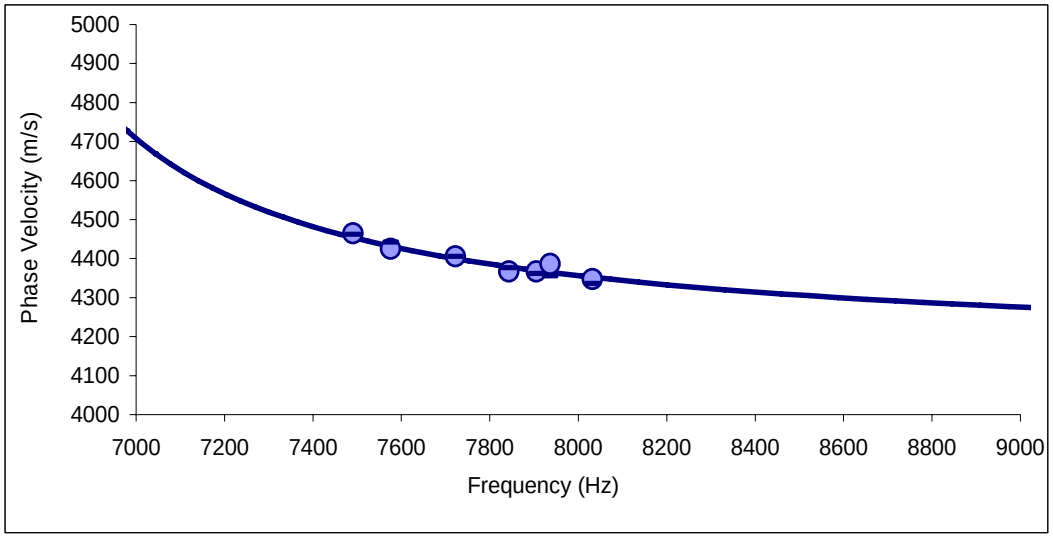

Figure 17: Fit of a typical set of experimental data (points) onto a theoretical S_1 phase velocity dispersion curve (line).

A screenshot of the main page of the VBA application designed for effective processing and computation of field data, with capabilities of importing and exporting to databases, is presented in Figure 18.

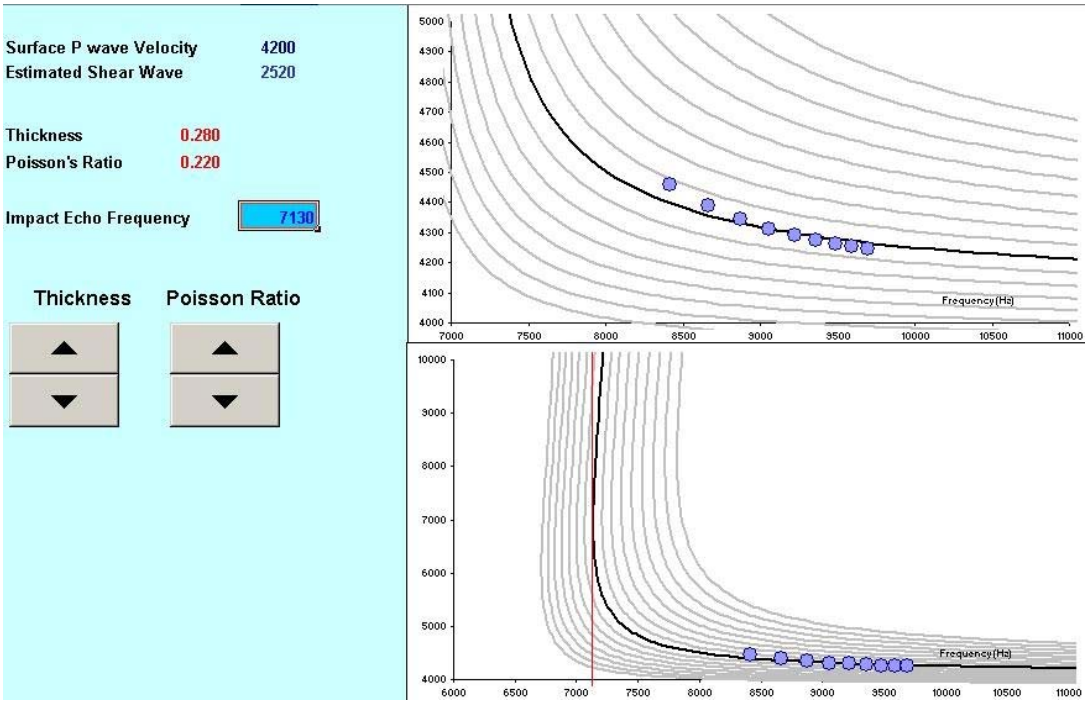

Figure 18: Screenshot of the VBA application developed to solve field data.

In-place Strength Determination

The objective of this work is to develop NDE techniques that can estimate accurately in-place strength of concrete regardless of composition or material conditions. The use of surface wave parameters is proposed for this purpose.

Design of Experimental Testing Set-up

Basic Concept

Concrete strength is known to be strongly related to the amount of capillary porosity, air voids, and microcracks distributed throughout the hydrated cement matrix and along the cement-aggregate interfaces. Higher levels of porosity give lower concrete strength (Mindess et al. 2003). Several factors, in turn, affect the amount of porosity such as w/cm ratio, concrete maturity, or environmental factors. Porosity, air voids, and microcracks affect propagating wave characteristics since they serve as good reflectors (scatterers) of propagating surface wave energy. Therefore, some of the wave energy will be dissipated by the scatterers present along the transmission path and, thereby, will result in lower energy transmission value. Wave velocity is related to the elastic constants of the material. Young's modulus, Poisson's ratio, and bulk modulus can all be related empirically to material velocities. Monitoring velocities allows estimation of elastic constants of materials and, indirectly, their strength (Bray and Stanley, 1997). Thus surface wave velocity and transmission are applied directly to monitor elastic constants and presence of these pore reflectors and, therefore, indirectly to estimate the strength of concrete.

Initial Testing Equipment: Controlled Impactor Source

In order to carry out these tests, a surface wave source, sensors, and data acquisition and analysis system is needed. The surface wave source is important since it determines the amplitude and frequency content of the waves. In the preliminary test series, a powered impactor manufactured by Develogic was applied as the surface wave source. This impactor is shown in figure 19. The impactor motion is based on high-speed stroke magnets, which allow for variable energy levels. It can be easily handled and has an output port that allows for impact time determination (Develogic, 2003). The approximate contact time of an impact is about 100 μs.

Figure 19: Automatic impactor (Develogic 2003).

The sensors were miniature accelerometers developed by PCB Piezoelectronics, model 352B10. These accelerometers have a sensitivity of 10.89mV/g at 100 Hz. Their resonant frequency is close to 80 kHz and the flat response range goes from 3 to 10000 Hz. A digital oscilloscope (LeCroy Waverunner, model LT344) was used to digitize the signal data. The digital oscilloscope gathers 10,000 points for each signal. The scope was connected to a rugged laptop computer via a GPIB connection, which was used to gather, analyze and store data. A computer program based on the LabWindows platform was used to acquire and process the data.

Follow-up Testing Equipment: Ultrasonic Transducer Source

The results from the preliminary testing series indicated some problems with the impact wave source, namely, high levels of incoherent (thermal) noise, inconsistent and low useable frequency contents. These problems resulted in undesired thickness and end-reflection responses that disrupt the transmission response. Thus a new ultrasonic (non-impact) source was investigated. The source is a point-contact ultrasonic transducer with a center frequency of 200 kHz, which is significantly higher than that provided by the impact source. The transducer excitation tip is made of a rubbery material, which allows effective source/concrete contact regardless of the surface roughness; these sensors enable rapid and practical measurements on any concrete surface without grease or gel couplant. The relatively high frequency is appropriate for the transmission tests, as preliminary work showed that low frequency transmission results (< 80 kHz) are disrupted by slab edge boundaries and guided waves set up through the slab thickness. The transducer is driven by a pulser unit having a high pulse repetition rate. A photo of the transducer sources is shown in Figure 20. Such a setup allows for the collection of 100 repetitions for each signal allowing signal averaging to significantly reduce the incoherent noise levels and thereby increase the signal to noise ratio in the signals. The rest of the testing

equipment (sensors, digital oscilloscope, computer, program, etc.) are identical to those used in the preliminary testing series.

Figure 20: Dry-contact point transducers used for surface wave tests in concrete. Transducer center frequency is 200 kHz.

Initial Work: Laboratory Specimens

In the preliminary test series, several 50cm x 50cm x 10cm concrete test slabs were cast. Several different concrete mixtures were selected in order to obtain a range of strengths (w/c = 0.4 to 0.52) and entrained air contents (either air entrained and non-air entrained). All mixtures were comprised of Type I Portland cement, crushed limestone (maximum size = 25mm) and river sand. The slump and air content were measured for each fresh mixture. Three accompanying 4 inch by 8 inch cylinders were cast along with each slab in order to determine the strength of the mixture by compression tests at 28 days.

Follow-up Work: Laboratory Specimens

Based on the findings of the preliminary experimental test series the follow up experimental test series was designed to evaluate the effectiveness of the developed surface wave velocity and transmission measurements, using the new ultrasonic wave source, to estimate in-place concrete strength. In the previous tests, only compressive strengths were measured. In this test series both compressive and flexural (modulus of rupture or MOR) strengths are

evaluated. A new set of concrete mixtures were designed and manufactured with a range of possible and realistic properties (varying w/cm ratio, aggregate types and cementitious materials types). All concrete mixtures satisfy 2005 Virginia DOT mixture specifications. The mixture properties are shown in Table 1. The mixtures with "L" designation contain ¾ inch crushed limestone coarse aggregate, and those having "T" designation have ¾ inch crushed trap rock. All mixtures contain entrained air. These two aggregates were selected to represent aggregates comprised of soft/compliant minerals (e.g., limestone) and hard/stiff minerals (e.g., trap rock). Mixtures with at least two different material MOR strengths (w/cm ratio) and two different compositions (aggregate type and/or content and cementitious material) are considered. The concrete mixtures were designed to simulate typical concrete mixtures used in Virginia. The concrete was supplied by a local ready-mix supplier. Compressive strength (cylinder) and MOR (beam) development for these mixtures is obtained from companion specimens, which are tested regularly up to the age of 28 days; tests were carried out at the ages of 1, 2, 3, 5, 7, 10, 14, 21 and 28 days after mixing. Three companion samples are tested at each age. At the same time, V_R and T_R are measured from laboratory slab specimens and the MOR beam samples themselves.

Table 1: Mixture proportions (relative to cement) and fresh properties for test slabs.

Designation	**L43**	**LF43**	**T43**	**T47**
Cement (I)	1.0	1.0	1.0	1.0
Fly ash (C)	---	0.32	---	---
Fine agg.	2.39	2.9	2.37	2.39
Coarse agg.	3.59	4.52	3.57	3.61
Water	0.44	0.57	0.44	0.46
Slump (mm)	70	76	44	76
Air content (%)	6.4	6.7	7.0	6.0
Unit wt. (kg/m^3)	2333	2387	2240	2300
w/cm	0.439	0.434	0.440	0.462

Analysis Approach

In order to determine transmission in concrete slabs, a self calibrating technique was used. This technique makes use of two wave sensors and two wave sources placed along the same line. When an impact is generated at point *1*, surface waves propagate along the surface and are captured by both the near sensor, located at *2*, and the far sensor at *3*. In the frequency domain, the signals that are sent from the impact source at location *1* and then detected by the receivers can be represented as a simple product of terms (Song et al. 2002):

$$V_{12} = S_1 d_{12} R_2 , \tag{12}$$

$$V_{13} = S_1 d_{12} d_{23} R_3 \tag{13}$$

where V_{12} and V_{13} are Fourier transformed signals, S_1 the generating response term, R_2 and R_3 the receiving response terms, d_{12} the signal transmission function between *1* and *2*, and d_{23} the transmission between *2* and *3*. The signal transmission function includes information about the geometric attenuation of the surface waves. The *S* and *R* terms also include information that is a

function of source and sensor coupling conditions, which are unknown. In order to eliminate these unknown effects a complimentary set of V_{43} and V_{42} signals must be collected. These signals are generated when a wave source is applied at location *4* and detected by the receivers at *3* and *2*. These may be again expressed as a product of terms (Song et al. 2002):

$$V_{43} = S_4 d_{43} R_3 , \tag{14}$$

$$V_{42} = S_4 d_{43} d_{32} R_2 . \tag{15}$$

We seek to isolate and measure the d_{23} term, which represents the transmission between *2* and *3*. By manipulating the V_{ij} terms the transmission T between the two sensors may be defined (Song et. al 2002):

$$T = \left| d_{23} \right| = \left| \sqrt{\frac{V_{13} V_{42}}{V_{12} V_{43}}} \right| . \tag{16}$$

Not all the data acquired may be used. There is a range of frequencies within which the data are useable. This is determined by the signal consistency function (SC), which is obtained from five repeated data sets 'd' at each location (Song et al. 2002):

$$SC(f) = \frac{\sqrt[5]{d_a d_b d_c d_d d_e}}{(d_a + d_b + d_c + d_d + d_e)/5} . \tag{17}$$

For this particular study, data at frequencies with SC $\geq$ 0.99 were considered to be acceptable (Popovics et al. 2000).

In the program for signal transmission computation, five repeated signal sets are collected, and the digitized signals are converted into the frequency domain with a Fast Fourier Transform algorithm. Each frequency signal is then analyzed by the user who sets a cursor and selects a point around which a Hanning window is centered. A Hanning window isolates important portions of the signal. Zero padding is then used to add zeros at the beginning and end of the signal. This process is used to increase sample length, and thus increase the resolution of the analyzed signal in the frequency domain. The signals are then processed to obtain signal consistency and transmission as described in Eqns. 16 and 17. Surface wave velocity measurements are obtained from two sensors spaced a known distance along a path on the surface of the specimen. A surface wave is launched close to one of the sensors and the time required for the signal to travel from the near sensor to the far sensor (Δt) is recorded. The ratio of the distance to the recorded time is taken as the surface wave velocity. Figure 21 shows the signals detected by the near and far sensors. The time lapse between the first significant signal features, in this case the first valley, of both is taken as the time of flight of the surface wave. (Cho 2003).

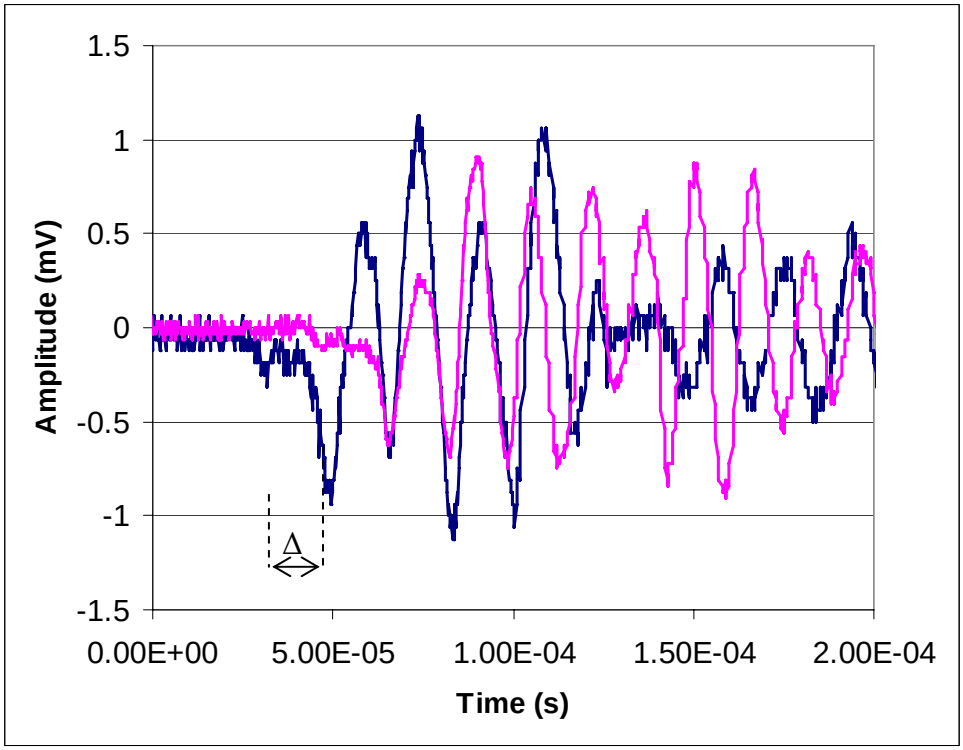

Figure 21: Surface wave signals from impact source. Black line is near sensor and gray line is far from sensor.

RESULTS

Pavement Thickness Determination

Frequency Domain Method

P-wave velocity measured by 1-sided and through-thickness methods at a selected core location for all three slabs, respectively, as a function of age were measured. As expected the slabs show some increase in velocity within the first several days after casting because of intensive hydration activity, leveling off to a relatively constant value by day 7. Slabs 2 and 3 exhibit a slight decease in velocity after day 30, likely because of internal drying over time in the dry laboratory air environment. Data collection on slab 3 could not be started until 7 days after casting. At all ages, the through thickness (UPV) velocity is significantly larger than the one-sided velocity. On average, 1-sided velocities are 300 m/s lower than UPV. This difference, which has been observed and confirmed by other researchers (Boyd and Ferraro 2005; Qixian and Bungey 1996, Jones 1962), is greater than that caused by velocity systematic error ($\Delta V = \pm$ 50 m/s), and therefore must have some other cause. The material property gradient in the drawn cores was established by measured UPV velocities through slab height, as measured from the individual sectioned slices of cores. The tests are carried out on the concrete disks in saturated moisture condition to eliminate any effects owing to internal moisture gradients. The velocity trends for each sequential disc as function of depth through the cores were measured, where disc 1 is the top and disc 5 the bottom of the core. Despite some data scatter, a trend of increasing

wave velocity with depth is seen; on average the wave velocity of the material increases 8% with slab thickness from the finished surface at the top (disc 1) to bottom (disc 5). The established gradient likely contributes to the discrepancy between velocity measured along the surface (mostly disc 1) and through the thickness (average of all discs).

Because of the observed velocity differences, the thicknesses predicted by impact-echo will vary depending on the velocity value applied. Figure 22 shows the predicted thicknesses for the three slabs, as a function of age, using both velocity values and assuming a β value of 0.952, which represents a typical expected theoretical value for concrete. Although the data show some scatter the values are fairly constant as a function of concrete age, so there is no clear influence of concrete age on the estimated thickness values. It is clear however that the thickness estimates are closer to the actual thickness (determined by core sample) at all ages when the through-thickness UPV is used with this value of β. The thickness estimates using 1-sided velocity are lower than the actual thickness in nearly all cases. Again, these differences are greater than that caused by system resolution error. To illustrate, the thickness estimates and errors for the two core locations in all three slabs were computed. Standard impact-echo using one-sided velocity under-predicts the slab thickness on average by approximately 10mm, while UPV over predicts by about 7mm. Significant variability in the thickness estimates is evident in both cases. The average squared thickness error for all slabs, core locations and ages is 7.8 mm for UPV and 13.2 mm for one-sided velocity, assuming β =0.952, both of which are beyond the desired accuracy limit of 6mm.

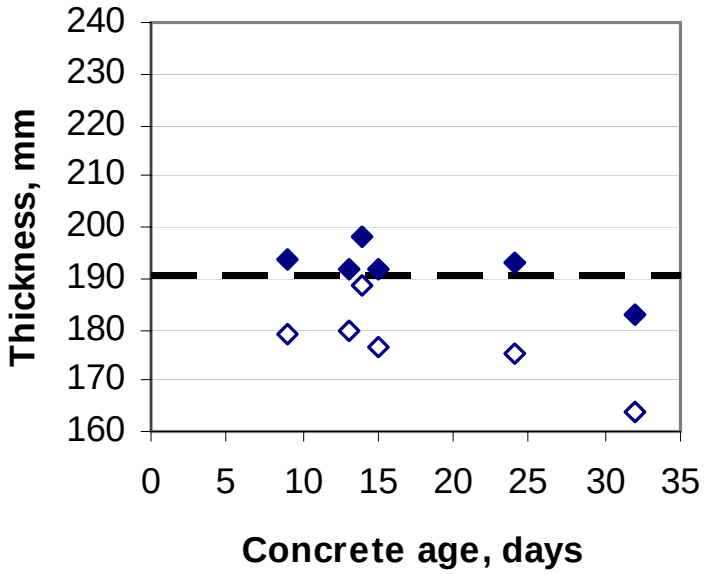

Figure 22: Predicted impact-echo slab thickness using through-thickness UPV (solid symbols) and one-sided wave velocity (hollow symbols) as a function of concrete age for a slab. Actual slab thickness (core) indicated by solid line.

By manipulating Equation1, β values can be back-computed using actual core thickness and measured values of P-wave velocity. β values obtained in this way are shown in Figure 23 for all core locations and slabs, using the two types of P-wave velocity measurement. The data

show a significant degree of scatter, and it is clear that the experimentally back-computed β values differ than the range of 0.945 to 0.955 that is theoretically predicted. In the case of 1-sided velocity, the β values are generally above 1 with an average value of 1.01, while for UPV the values are lower, generally below 1 with an average value of 0.935. These differences are due only to the method of wave velocity measurement, as consistent resonance frequency values were used, so the scatter in the data is a result of variability in wave velocity data rather than that in the resonance frequency data. The resonant frequency values showed excellent consistency upon repeated tests.

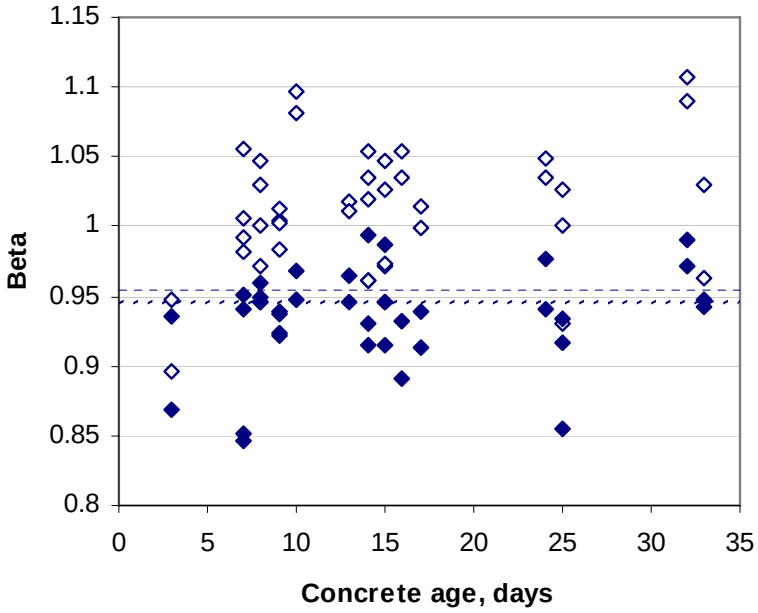

Figure 23: Back-computed β values using through-thickness UPV (solid symbols) and one-sided velocity (hollow symbols) obtained from all slabs and core samples. Theoretical limits of β values indicated by dashed lines.

Hybrid Method (Seismic/Impact-echo)

The described seismic reflection procedure was carried out on the cast test slabs. Estimated thickness values were calculated by fitting experimental phase velocity dispersion to the Rayleigh-Lamb solution and then minimizing the error with regard to thickness and Poisson's ratio for an assumed C_P.

A full routine of non-destructive tests was repeated at 4-day intervals between 5 and 28 days after casting, at which time cores were extracted in order to provide ground-truth thickness values and axial C_P obtained by ultrasonic pulse velocity (UPV) measurements. Testing was performed along a 2m line on the longer centerline of the top face of each slab, as indicated in Figure 24, at a sufficient distance (at least 10 cm) from the edges of the slab to eliminate

unwanted reflections from the lateral boundaries. Five cores were taken from each slab, at 25 cm spacing along the testing centerline as indicated by the circles in Figure 24**.**

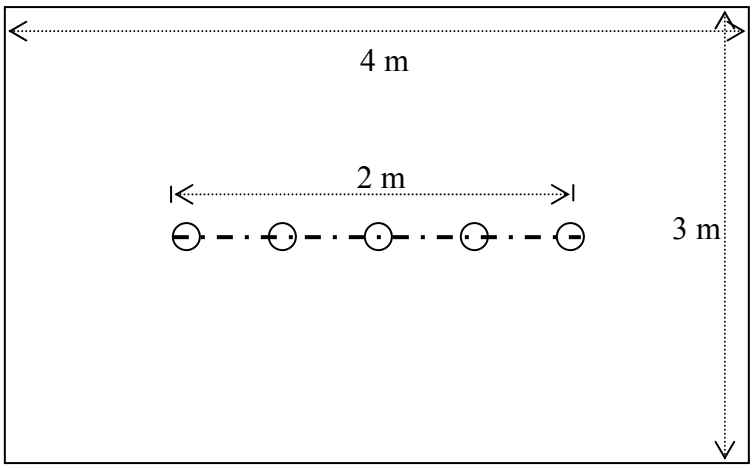

Figure 24: Test slab plan view, indicating the test line and location of cores.

Impact-Echo frequency measurements were obtained using a commercially available system, with a displacement transducer and PC-based data acquisition and processing. Seismic reflection measurements were performed using an impact source, two accelerometers and a multi-channel digital oscilloscope. The impact source consisted of a 4.5 mm caliber spring powered BB-gun with a muzzle velocity of approximately 67 m/s, described in detail in the previous chapter. The end of the barrel was held at a fixed distance of 75 mm (3 in) from the surface by means of an acrylic casing, which provided both impact force consistency and safety. The out-of-plane response was measured by two miniature accelerometers (PCB Piezotronics 352B10) which have a resonance frequency of approximately 65 kHz. (see Figure 25) Measured signals were digitalized and recorded at 10 MHz, equivalent to one sample every 0.1 microseconds, recording a total of 10000 points.

Figure 25: Experimental setup for the seismic reflection test.

At the time the slabs were cast six 12 x 6 inch control cylinders were made and were maintained on site under similar conditions as the slabs. At 28 days the ultrasonic pulse velocity was measured. In addition to UPV, dynamic Poisson's ratio was measured (Kolluru et al. 2000), and finally 28-day compressive strength was determined by measuring the ultimate axial compressive load capacity.

The thicknesses of the three slabs were nondestructively estimated using the new hybrid method and the conventional impact-echo method. The experimental setup for seismic reflection testing was placed along the centerline of the slab, as indicated in the sketch in Figure 24. The two accelerometers were placed at a fixed spacing of 50 cm, and a set of impact locations arranged so as to cover the distance equivalent to 4h to 8h from the far accelerometer. Two sets of measurements were taken per slab, by switching the relative position of sensor and impact locations. Along the same testing line, 21 Impact-Echo frequencies were collected at 10 cm intervals. Impactor sizes were selected in order to optimize frequency input according to the resonance frequency of each slab. The dynamic response was sampled at a rate of 2 μs per point, with a total of 2048 (2^{11}) points. In order to increase frequency-domain precision the recorded time-domain were zero-padded to a total of 2^{15} points prior FFT processing, yielding a frequency resolution of 15.26 Hz. Seismic reflection and IE measurements were repeated 7 times on each slab at 4-day intervals, between 5 and 28 days after casting.

The tests were carried out regularly over a span of several weeks after the slabs were cast. Test results from days 8, 16 and 28 after casting are presented here. The average depth of five cores taken on day 28 from each slab is shown as the actual thickness value. Table 2 displays the results for the impact-echo method and Table 3 from the new hybrid method. The thickness predictions from the conventional impact-echo method are shown to remain within 4% of the actual thickness, with an average error estimate of 6.2 mm and a maximum error of 10 mm. There is no clear consistent trend in the thickness predictions over time as the concrete matures. The performance of impact-echo is reasonably good, but on average it does exceed the established ±6mm thickness accuracy requirement.

Table 2. Actual (core) vs. predicted impact-echo thickness values for 3 test slabs. Average error for all tests is 6.2 mm.

Slab	Actual Thickness (mm)	Impact-echo predicted values (mm)					
	(core on Day 28)	Day 8		Day 16		Day 28	
		prediction	error	prediction	error	prediction	error
S20	235	236.0	1.0	239.8	4.8	241.1	6.1
S25	276	280.6	4.6	281.9	5.9	286.0	10.0
S30	310	316.8	6.8	319.7	9.7	316.5	6.5
Percent Error Range Per Day		0.4% - 2.2%		2.0% - 3.1%		2.1% - 3.6%	

The results show that the hybrid seismic impact-echo method does provide better estimates of average concrete slab thickness than conventional impact echo. The thickness predictions from the new hybrid method are also remain within 4% of the actual thickness and the average error estimate is 4.0 mm, well below the established ±6mm thickness accuracy requirement. There is no clear consistent trend in the thickness predictions over time as the concrete matures, although the estimate error increases with the actual pavement thickness. The performance of new hybrid method is satisfactory, clearly meeting the performance requirements.

Table 3. Actual (core) vs. predicted hybrid method thickness values for 3 test slabs. Average error for all tests is 4.0 mm.

Slab	Actual Thickness (mm)	Hybrid method predicted values (mm)					
	(core on Day 28)	Day 8		Day 16		Day 28	
		prediction	error	prediction	error	prediction	error
S20	235	236.0	1.0	238.5	3.5	244.0	9.0
S25	276	280.0	4.0	275.5	-0.5	282.0	6.0
S30	310	308.5	-1.5	314.5	4.5	316.0	6.0
Percent Error Range Per Day		0.4% - 1.4%		0.2% - 1.5%		1.9% - 3.8%	

In order to study the possible disrupting effects of steel reinforcement and internal objects (tendon ducts) within the concrete on the hybrid test method, verification tests were subsequently performed. The hybrid test was carried out on a mature 258 mm thick steel-reinforced concrete slab with thickness ranging from that contains two internal tendon ducts that run the length of the slab. The slab contains a square grid of #4 bars (12mm diameter) with a 250mm bar spacing. A drawing of the test slab is shown in Figure 26. The tests were carried out along a line which runs over the internal ducts, ensuring some interaction between the wave pulses, internal ducts and steel reinforcement. The collected hybrid test data were of good quality, and apparently not-disrupted by the steel reinforcement and internal ducts. The test results are shown in Figure 27, where it is seen that that the seismic data points collected from the different impact locations are consistent. Impact Echo tests exhibited an average frequency of 7900 Hz. Using the hybrid approach, the impact echo frequency and seismic data points yielded a predicted thickness of 264 mm and concrete Poisson's ratio of 0.17. This results in a

thickness error of 6 mm. This level of accuracy is (estimate approximately 2% of thickness) is good and encouraging, especially considering the significant amount of steel and embedded ducts in the slab.

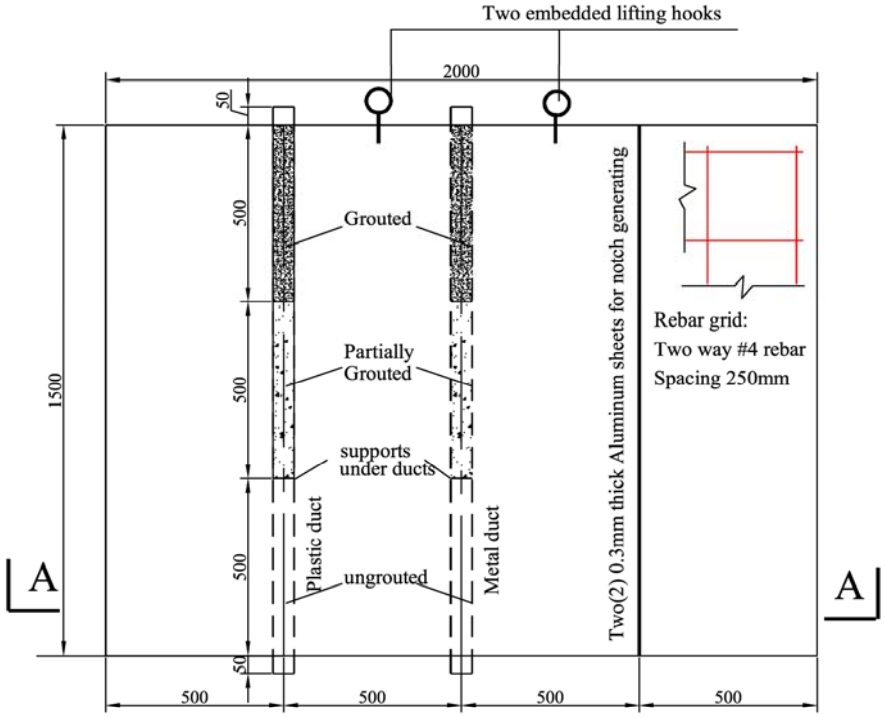

Figure 26: Drawing of reinforced concrete test slab that contains internal defects. All dimensions in mm. Hybrid tests carried out along a line which runs over the internal ducts.

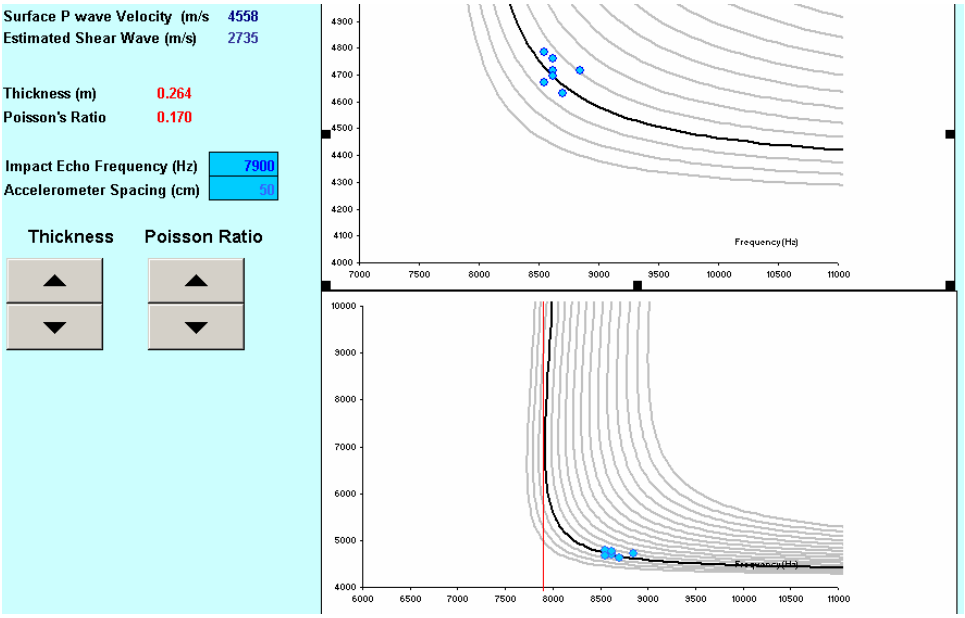

Figure 27: Screen shot of hybrid test results from reinforced slab containing internal ducts. The analysis predicts a slab thickness of 264 mm.

In-place Strength Determination

Preliminary Test Series

A preliminary test series was carried out to determine the feasibility of using surface wave velocity and attenuation measurements to predict concrete strength. Full detain on this study can be found elsewhere (Gallo and Popovics 2005). The principal findings are summarized here.

Concrete compressive strengths were determined from cast companion cylinders. Strength generally decreases with higher water/cement ratios, as expected. Also, strength increases with maturity. In addition it is seen that the richer mix has the largest compressive strengths. This is also attributed to differences in air content and compaction. In general, there is a clear trend among all groups: larger air contents yield lower compressive strengths. This also verifies that the mixes with constant water/cement ratio have differences in compressive strength due to variations in air content.

Through thickness P-wave velocity (UPV) measurements were performed at three different locations on each slab, with two test repetitions at each location. The distance between the transducers (slab thickness) was measured with a caliper. Errors may be introduced in the procedure by the measurement of the travel distance, since local variations were difficult to account for with the caliper.

Surface wave velocity measurements were taken with a sensor spacing of 0.2m. Three locations on the slab were randomly selected to minimize the effects or variation in velocity due to local conditions along the wave travel path; the average value was reported. For the first two sets of slabs, surface wave velocity measurements were taken on both the upper (trowelled) and lower (formwork) faces. Velocity results on the bottom cast face were found to be consistently higher than those on the upper trowelled finished face. Finishing alters the surface properties since floating and trowelling leave behind a modified surface. In the process, aggregate particles are embedded beneath the surface leaving a richer zone on top (Kosmatka and Paranese 1994). This may explain the differences in the results, as the finished surface has lower aggregate content along the testing path. For each slab, 5 lines were selected along which transmission measurements were collected. Three of these lines were evenly spaced in one direction. The fourth line was perpendicular to these three in the middle of the slab and a final inspection line was drawn diagonally form one corner to the opposite one.

Transmission data were collected on the upper and bottom faces of the first two sets of slabs with 5 cm sensor spacing. In the remaining slabs only the bottom, or formwork side, was tested. Transmission was studied at two frequency ranges, from 15 kHz to 30 kHz and from 116 kHz to 130 kHz. These regions were selected based on the obtained transmission data. Within

these regions all the transmission functions obtained for the specimens were relatively flat, with acceptably high signal consistency.

The graphs in the figures reveal that the air and non-air entrained slabs show similar transmission at lower frequencies for the upper and bottom face measurements. At higher frequencies the transmission is similar but there are some differences. Non air-entrained slabs tend to have higher transmission values along the formwork faces compared to the trowelled faces. This difference is not significant in the air-entrained slabs. Transmission increases with concrete age. This difference is not as marked at lower frequency ranges but is clear at higher frequency ranges. However, at higher frequencies there are missing sections of data due to unacceptable signal consistency. Transmission is higher for the richer mix and lower for the lean mix within most of the frequency ranges.

Correlation to Strength

After all experiments were carried out, combinations of data were used to investigate correlations with concrete's compressive strength. Linear, second order polynomials, exponential, and power relations between strength and NDE parameters were investigated. The quality of each correlation was determined by the square root of the average squared errors:

$$error = \sqrt{\frac{\sum_{i=1}^{n}\left(f'c_{i-predicted} - f'c_{i-measured}\right)^2}{n}} \tag{18}$$

where n is the total number of data points, $f'c_{i\text{-}predicted}$ is the predicted compressive strength for a given correlation at a particular value, and $f'c_{i\text{-}measured}$ is the actual compressive strength obtained from companion cylinders. All concrete types and ages were considered together in a single regression.

Correlation between compressive strength and UPV, a common NDT approach, gave fairly good results with a simple linear fit, as shown in Figure 28. The average error (Eqn. 18) was calculated to be 6.76 MPa. The data, however, show some spread and moreover, the sensitivity of the approximation is only 13%. Sensitivity here is defined as the relative change (decrease) in the selected NDE parameter with respect to full range of compressive strength values. For the case in Figure 28, it is the relative change from the maximum UPV value to the lowest.

A similar approach is taken for surface wave velocity and transmission. Surface wave velocity shows sensitivity similar to that of UPV, although this average error was less: 5.92 MPa. Figure 29 shows compressive strength compared to surface wave velocity data; sensitivity is shown also to be 13%. Transmission shows the largest sensitivity, but at the same time the largest error: 10.4 MPa. Figure 30 shows that the sensitivity of transmission data is 36%.

Alternative approaches were investigated to better predict the compressive strength of concrete. First, data were normalized to simplify data merging. In some cases the normalized data raised to the tenth power and combinations of transmission and surface wave velocity were studied. The aim was simultaneously to reduce data spread and increase sensitivity. Table 4 shows the errors found with the different fits for each particular parameter. The column marked 'ACI' represents the power function approach described in ACI 228. In this approach the natural logarithms of the cylinders compressive strengths are plotted against the natural logarithms of the in-place test results. A linear relationship is then used to relate them and also serves to calculate errors (ACI, 2003).

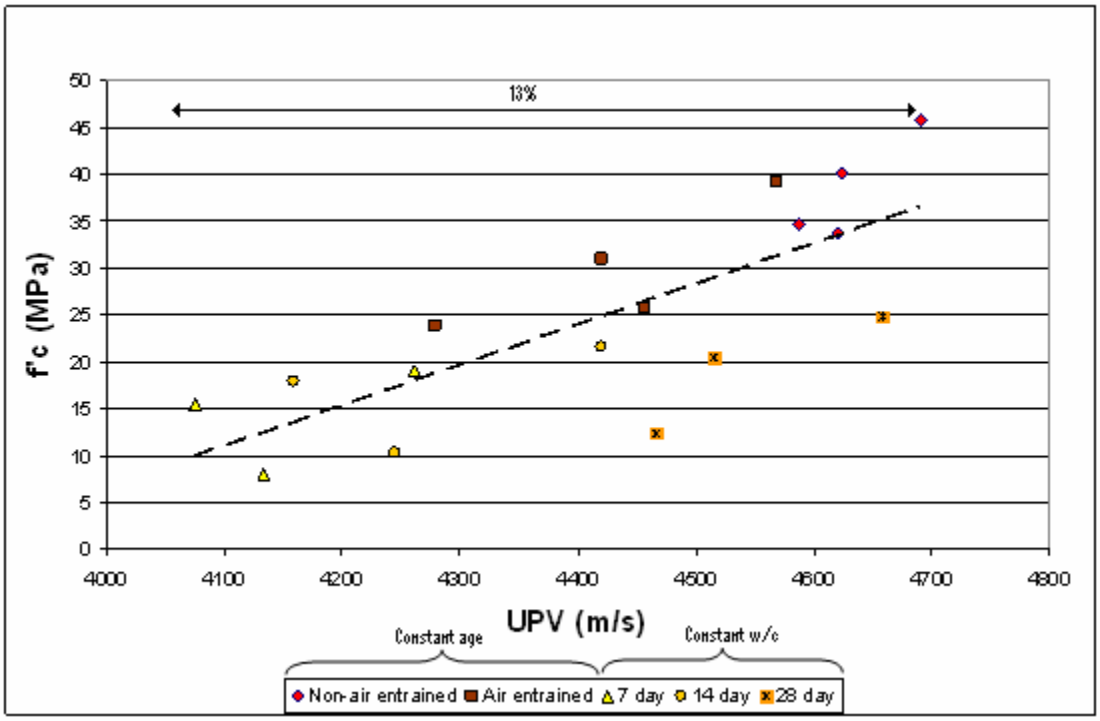

Figure 28: Compressive strength vs. UPV data (points) with linear best fit line.

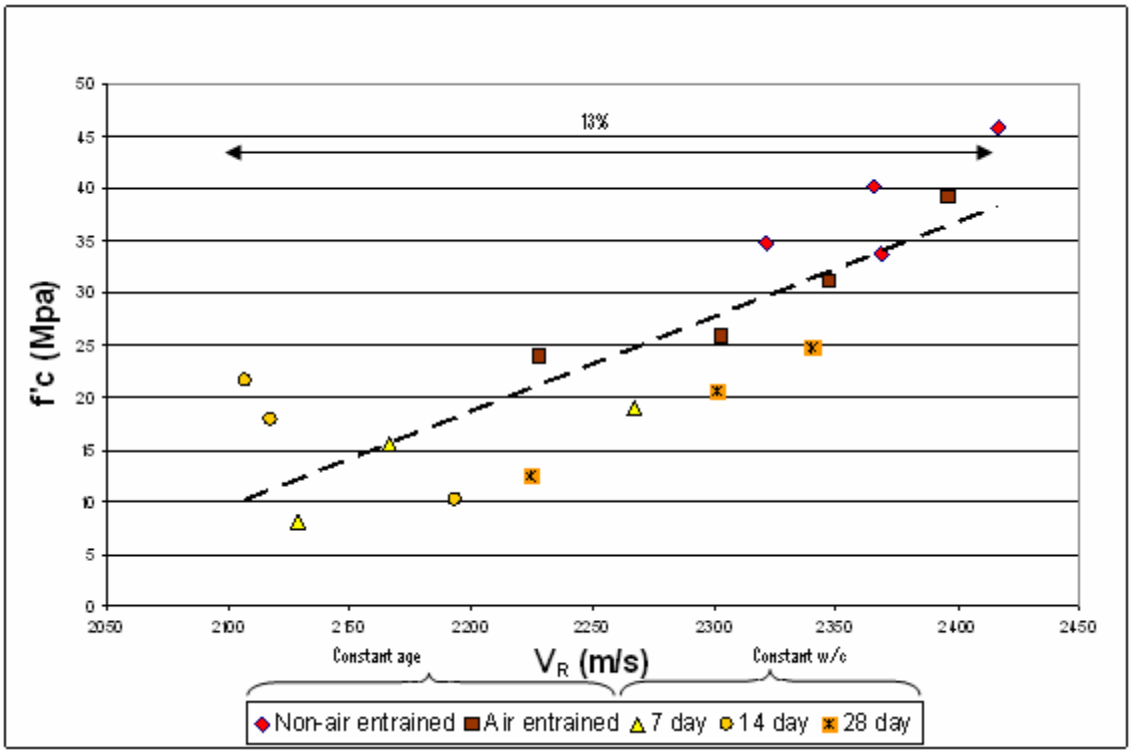

Figure 29: Compressive strength vs. surface wave velocity data (points) with linear best fit line.

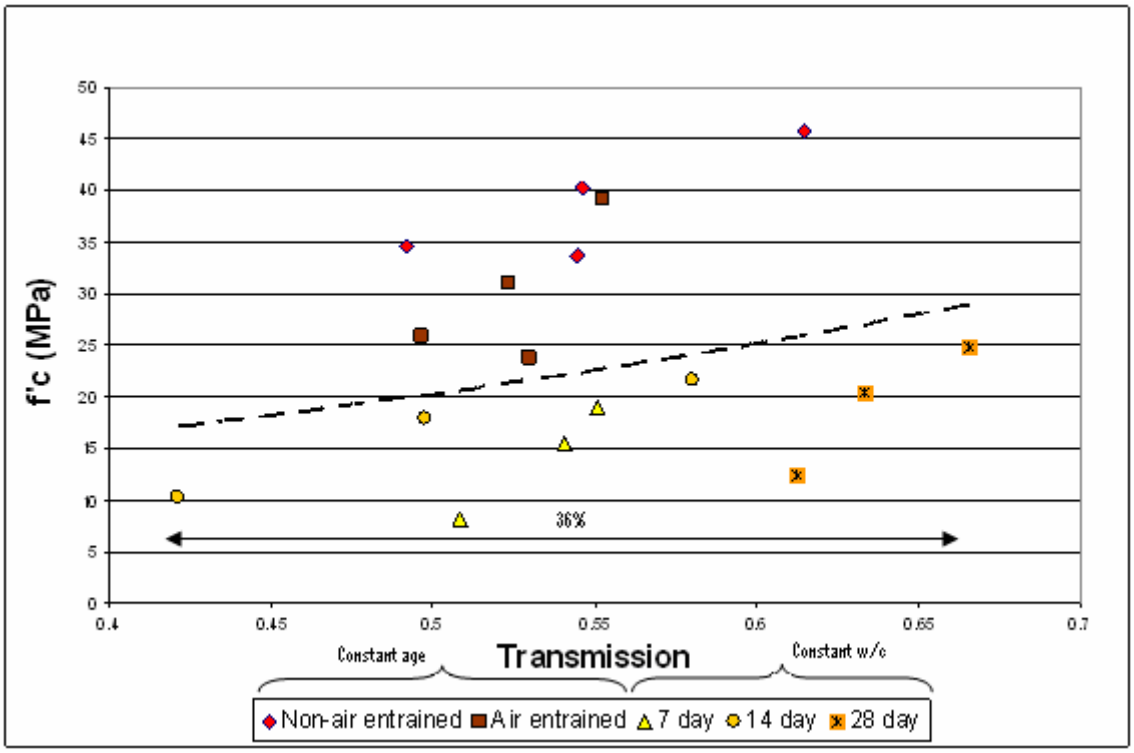

Figure 30: Compressive strength vs. transmission data (points) at high frequency range with linear best fit line.

Table 4: Average squared errors and for different fits. Sensitivities have also been included.

NDE Parameter	Error (MPa)				Sensitivity
	Linear	2nd order Polynomial	Exponential	ACI	(%)
Norm. Transmission	10.4	9.9	10.8	10.7	37
Norm. V_R	5.9	4.3	5.3	5.3	13
Norm. UPV	6.8	6.5	6.6	6.6	13
Norm. Transmission ^ 10	10.7	10.5	10.9	10.7	99
Norm. V_R ^ 10	5.0	4.6	4.7	5.3	75
Norm. UPV ^ 10	6.5	6.5	6.6	6.6	76
(Norm. T + Norm. V_R)	9.2	8.9	9.7	9.6	21
(Norm. T + Norm. V_R) ^ 10	7.4	7.2	7.9	7.4	76

Table 4 shows that surface wave velocity measurements give the best correlation to strength (least error). When this data set is raised to the tenth power, error is further reduced in most cases. There are slight differences among fits; 2nd order polynomial fit gives the best overall results. The ACI method gives errors consistent to those of the other fits. Combined data do not give improved results when compared to the small errors observed with V_R alone. Sensitivity was found to be largest for transmission data. The best balance of low error and high sensitivity are achieved by the normalized surface velocity raised to the tenth power.

Alternative approaches were investigated to better predict compressive strength within each group, where fits were applied to each individual mixture group. Normalized data and their combinations were again studied with linear, 2nd order polynomial, exponential, and power fits. The error was sharply reduced when models were fit to data from each sub-group. This result is not unexpected since it is usually easier to fit models to fewer data. Previously, the error was, on average, 7.7MPa for the general fits. The error is reduced on average to 2.2MPa, when fits are applied to data from each particular subgroup. The average error of linear, 2nd order polynomials, exponential, and power fits were comparable.

Another important result of the analysis within each mixture group is that the strength-prediction models based on transmission data, or combinations of transmission and surface wave velocity data, have in fact less error. For instance, a linear fit of transmission data measured at 7 days and raised to the tenth power for the slabs with constant water/cement ratio gives an average error of 0.1MPa. Before, when all data points were used, transmission-based predictions had the largest error. Within each group, however, transmission-based models are equally good, or even better, than those predictions carried out with the other parameters. Transmission data could therefore help in strength prediction within each group.

Ultrasonic Transducer Source

A follow-up test series was carried out to establish the viability of using ultrasonic point transducers instead of an impact source of waves. This approach was tried in an effort to overcome some problems inherent to the impact wave source, namely high levels of incoherent (thermal) noise, inconsistent and low useable frequency contents giving undesired thickness and end-reflection responses that disrupt the transmission response.

Ultrasonic tests were applied to the concrete mixture series described previously. Compressive and flexural strengths were determined from cast companion cylinders and beams, respectively. Both compressive and flexural strengths were found to be higher overall for the limestone mixtures. This is clearly observed in Figures 31 and 32. The effect of changing w/cm on strength within the same aggregate type was not as significant. The higher compressive strengths may be attributed to better compaction, since the higher trap rock mixture with low w/c ratio was harsh, requiring more energy to finish and compact.

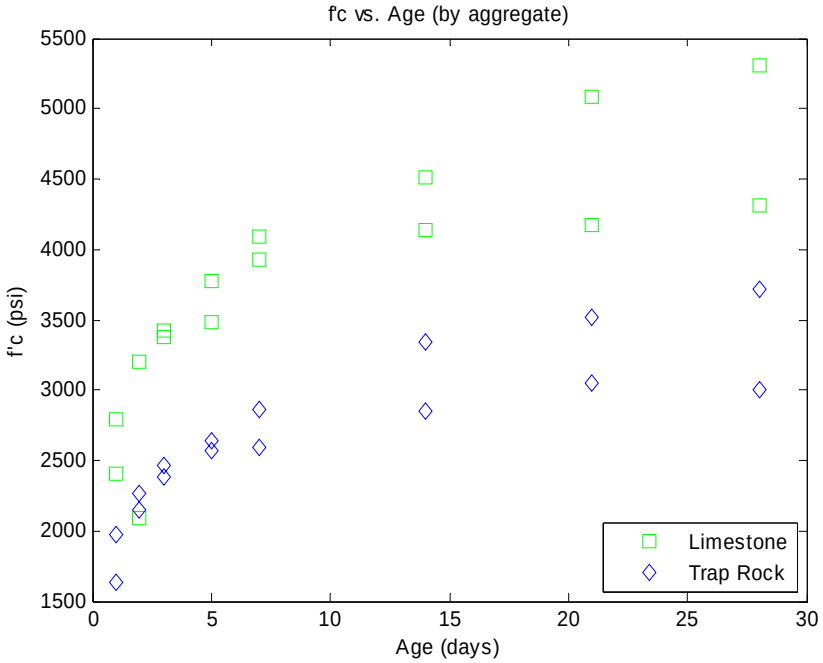

Figure 31: Compressive strengths as a function of age by aggregate type.

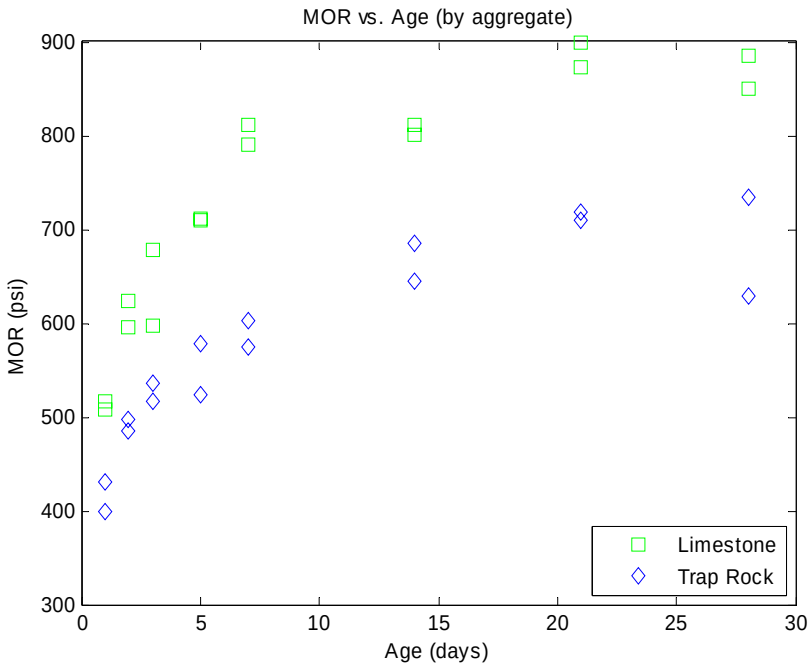

Figure 32: Flexural strengths (MOR) as a function of age by aggregate type.

Surface wave velocity measurements were taken with sensor spacing ranging from 2 cm to 10 cm at intervals of 1cm. At each location, the ultrasonic point transducer was placed 2cm from the near sensor. The slope of the line relating arrival times with distances was used as the velocity. Figure 33 shows a picture of the setup used for surface wave velocity measurements. Surface wave velocity measurements were taken on both the upper (trowelled) and lower (formwork) faces of all specimens. In general, velocity results on the bottom cast face were found to be higher than those on the upper face.

Figure 33: Testing configuration of sensors and point transducer on a concrete slab for surface wave velocity measurements.

Transmission data also were collected on the upper and lower faces of all specimens. Again, in general, transmission values on the lower surface were higher than those of the upper (trowelled) surface. Transmission was computed at two frequencies: 100 kHz and 220 kHz. Values at these two frequencies can be obtained from a single measurement since the computations are carried out in the frequency domain, and the transmission consistently had acceptably high signal consistency at those frequencies.

Ultrasonic velocity and transmission measurements from the cast surface (top) of beam specimens are used in the subsequent analysis, since this surface better represents the exposed surface of a concrete pavement. The ultrasonic tests were carried out on a beam specimen, which was then loaded in flexure until failure to obtain MOR. The obtained data reveal that surface wave velocity and transmission increase with concrete age consistently, as shown in figures 34 through 36. Surface wave velocity showed the greatest variation by mixture type. Transmission results showed much tighter correlation with age, regardless of the aggregate type. Transmission values at 100kHz show a slight differentiation between aggregate type, being the values for trap rock slightly higher than those for limestone.

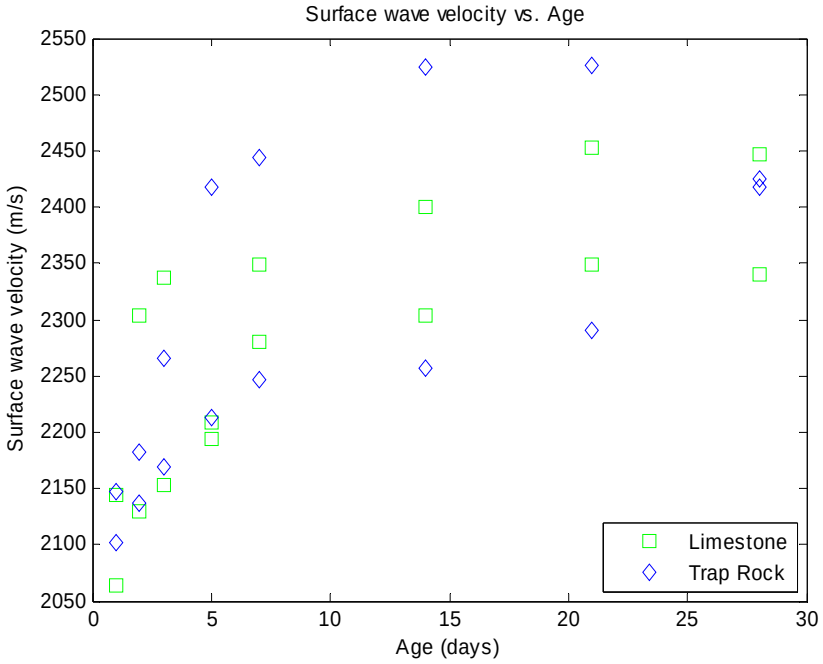

Figure 34: Surface wave velocity (m/s) as a function of age by aggregate type.

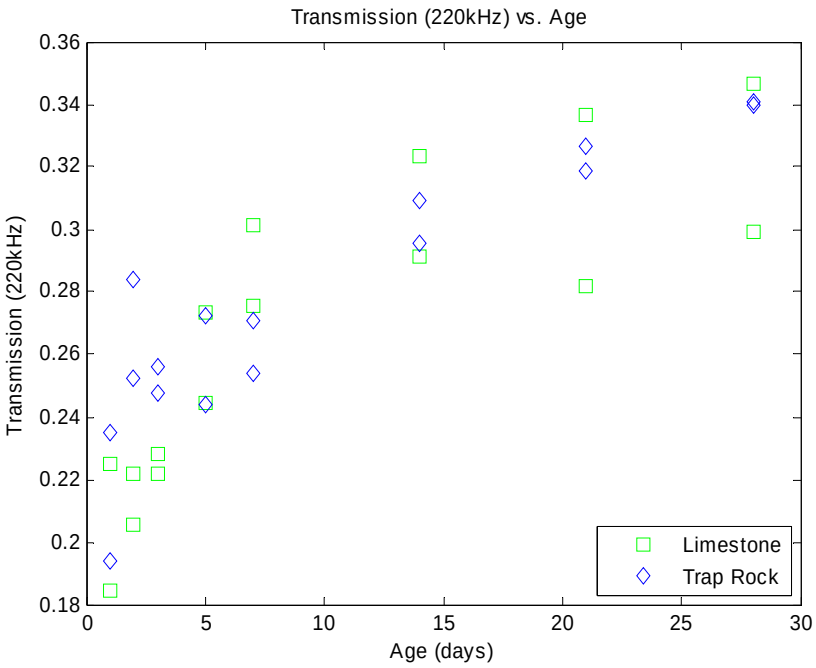

Figure 35: Transmission at 220kHz as a function of age by aggregate type.

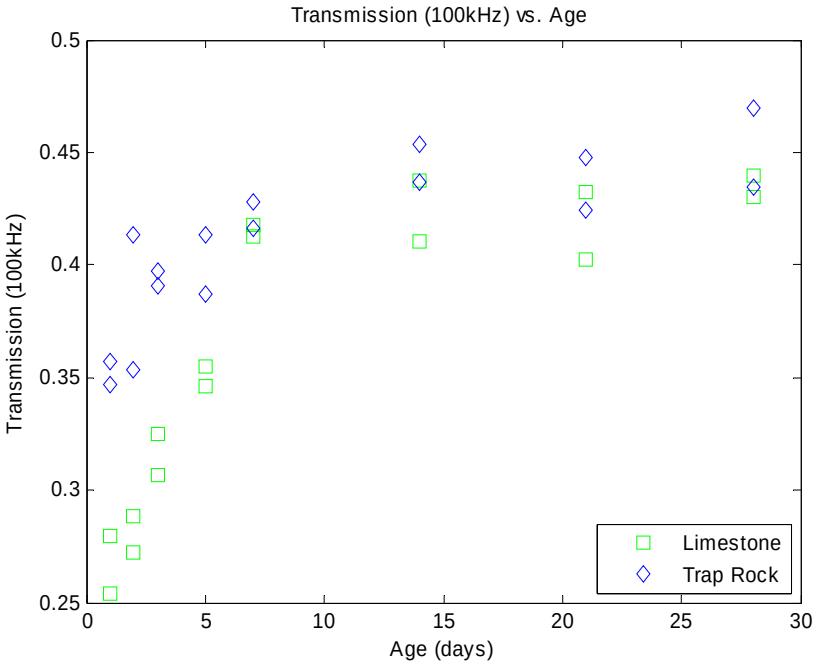

Figure 36: Transmission at 100 kHz as a function of age by aggregate type.

Correlation to Flexural Strength

After all the ultrasonic and strength tests were carried out, the data was analyzed for correlation between the ultrasonic parameters and flexural strength. Also, mathematical correlation equations which relate the strength to ultrasonic test parameters were proposed. The

effectiveness of an established correlation equation was determined by the square root of the average squared errors (Eqn. 18) between the equation and actual data. Figure 37 shows typical test data with best-fit linear correlation equations. Here MOR is correlated to signal transmission computed at 100 kHz. A clear distinction in behaviors between the two types of aggregate is seen in the plot. Within each aggregate type, the correlation between MOR and T_{100} is good. The best-fit line equations are for limestone

$$MOR = 1819.8 \times T_{100} + 68.015 \tag{19}$$

and for traprock

$$MOR = 2547.9 \times T_{100} - 467.59 \tag{20}$$

The average squared error for Eqn. 19 (limestone aggregate) is 44.2 psi and that for Eqn. 20 (trap rock aggregate) is 41.8 psi. These values of squared error are within our target accuracy goal of ±50 psi. However if all concretes are considered together regardless of the aggregate type, the average squared error increases dramatically to an unacceptable value of 104.9psi

Given that a significant distinction in behavior between aggregate types exists, two methods for in-place MOR prediction are proposed to overcome the problem of unknown aggregate type: (i) tests relative to known 1-day strength and ultrasonic values regardless of aggregate type and (ii) a two-step procedure based on signal transmission measurements at two frequencies: 100kHz and 200kHz; the first step is used to distinguish aggregate type (hard vs. soft) and the second for improved strength prediction within an aggregate type.

In the first approach, ultrasonic test results at a given age of concrete are compared to known 1-day values of the same ultrasonic parameter and the MOR collected at the same testing location. It was found that this approach resulted in good correlation (low average squared error) between ultrasonic parameters and flexural strength regardless of the aggregate type. Several different fit relations were evaluated, and the results are summarized in Table 5.

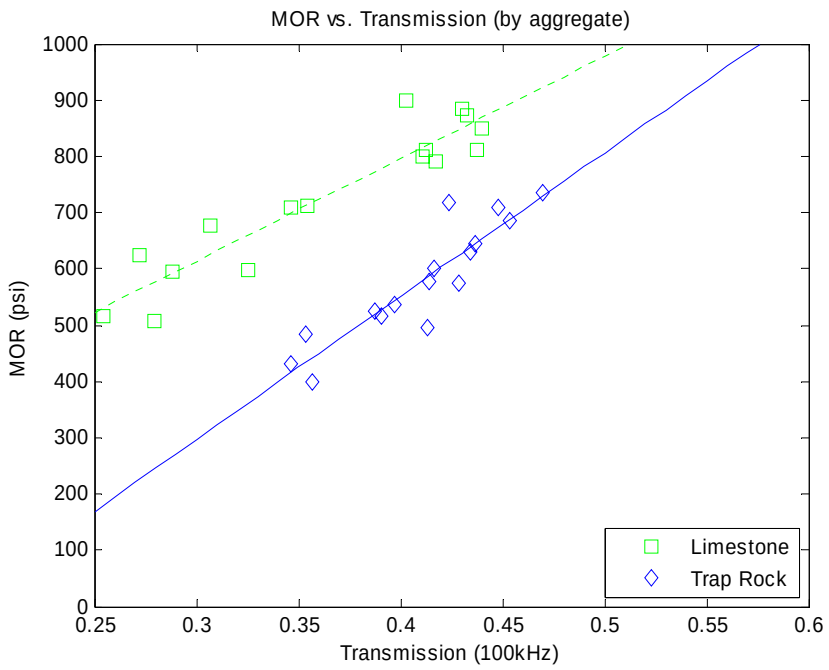

Figure 37: MOR as a function of signal transmission at 100kHz by aggregate type. Lines represent linear best fits to data within each aggregate type: Eqn. 19 for limestone and Eqn. 20 for trap rock.

Table 5: Average squared errors for different fits between NDE parameters normalized to the 1- day value and flexural strengths normalized to 1-day value.

NDE Parameter	Error (psi)		
	Linear	Linear (forced through 1)	2nd order polynomial (forced through 1)
Norm. Transmission	47.95	55.40	50.33
Norm. V_R	64.38	66.46	58.99

The best results are obtained when normalized transmission measured at 220 kHz (T_{220}) is linearly related the normalized flexural strength. The values at 1 day for both transmission at 220 kHz (T^*_{220}) and flexural (MOR*) at that same locations are needed for normalization. The value can be estimated by the following equation:

$$MOR_t = \left[\left(\frac{T_{220}}{T^*_{220}}\right) \times 0.9095 + 0.2348\right] \times MOR^*. \quad (21)$$

The average error for Eqn. 21 considering all tested specimens and aggregate types was 47.95 psi. This approach provides MOR estimates that satisfy the prescribed accuracy limit of ± 50 psi. A limiting aspect of this approach is the requirement for 1-day strength at ultrasonic values from the test location.

In the second approach, 1-day strength and ultrasonic test values are not needed. In the first step of this approach, transmission values at 100 and 220 kHz are used to distinguish between hard and soft aggregates. As shown in Figure 38, reasonably good distinction is achieved between the two aggregate types when the ratio of transmission measured at 220kHz to that at 100 kHz (T_{220}/T_{100}) is compared to T_{100}. Concrete with soft limestone aggregates have higher transmission ratio for a given T_{100} value than concrete with trap rock. A decision line that reasonably separates these two regions is given by:

$$\frac{T_{220}}{T_{100}} = 1.2 \times T_{100} + 0.2. \tag{22}$$

For a given ultrasonic test set, if the left hand side of Equation 22 is greater than the right hand side, then Equation 19 is applied to predict MOR; otherwise, Eqn. 20 is used to predict MOR.

When this two-step procedure was applied to all specimen data without distinction between aggregate type, the average squared error was 104.9psi. This level of average error is well above the defined target value of 50 psi.

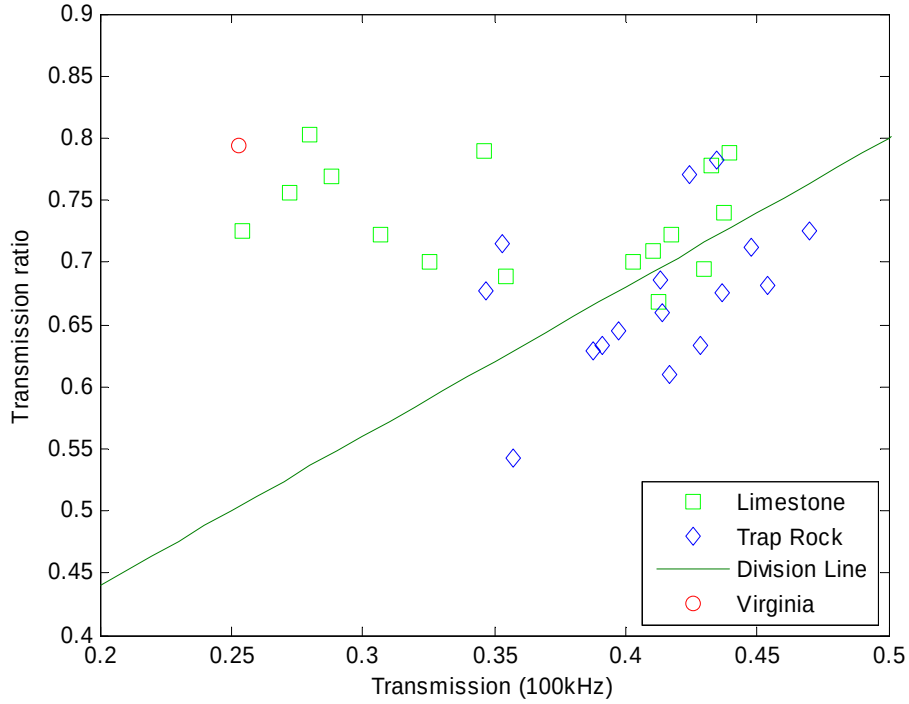

Figure 38: Transmission ratio as a function of transmission at 100kHz by aggregate type. The plotted decision line is given in equation 21. Appropriate flexural strength estimation equations (Eqns. 19 and 20) should be applied for each region.

Application to Asphalt Concrete Pavements

The developed pavement thickness approaches were applied to full-depth asphalt pavement sections. The tests were carried out in order to ascertain the viability of the approach for such pavements, as requested by VTRC research staff. The test developed for in place strength was not applied since the compressive strength parameter is not appropriate for visco-elastic flowing materials such as asphalt concrete. The tests were carried out on the morning of October 11, 2005 at the University of Illinois ATREL research facility (see Figure 39). The weather was overcast with an air temperature of 13-15^{o}C during the tests. The ATREL facility houses several sections of full-scale test pavement. The tests were applied to two sections of full-depth asphalt concrete pavement: a 420 mm thick (including all AC layers) section on compacted granular material, and a 255mm thick (including all AC layers) section on lime-stabilized soil. Both the seismic (time domain) and modified impact-echo) frequency domain were applied. For the seismic tests the BB gun was used as the wave source, and miniature accelerometers (same characteristic as in earlier tests) used as the sensors. For the impact-echo tests, a steel sphere (10mm diameter) was used as a wave source and standard displacement transducers was used as the sensor.

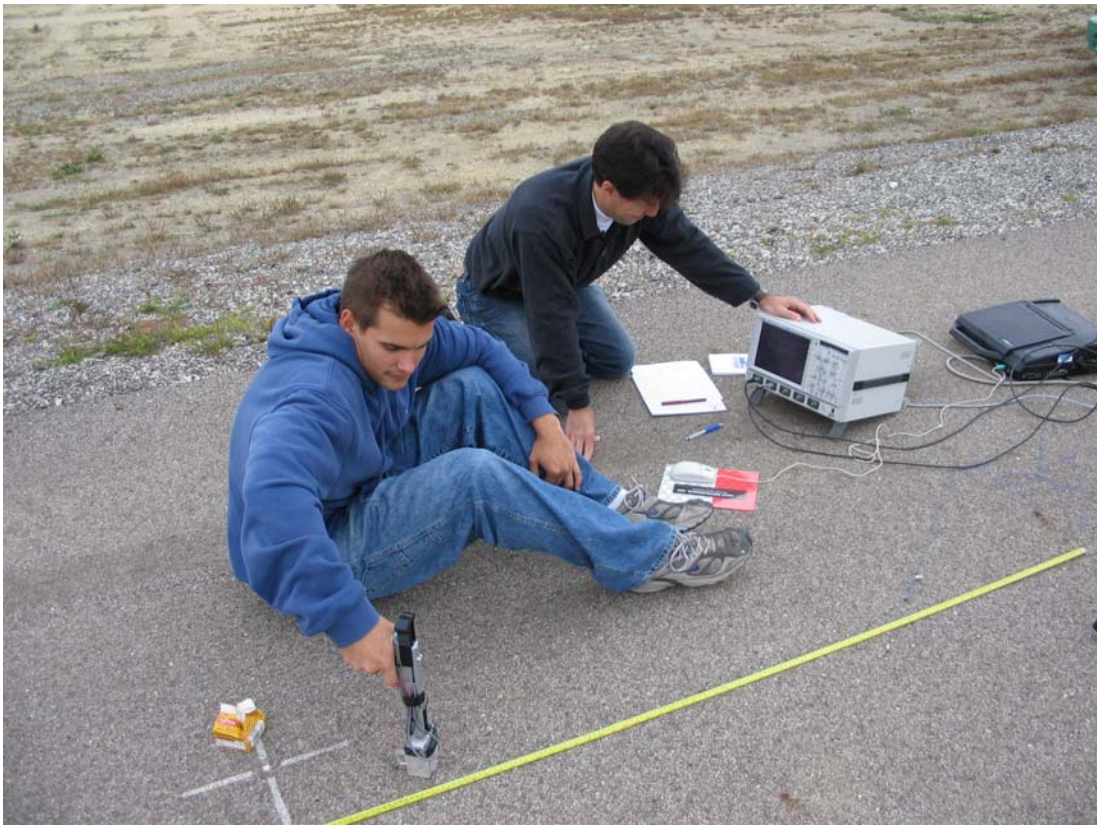

Figure 39: Application of seismic method to full-depth asphalt pavement at ATREL test facility.

For the 420mm thick pavement section, source receiver spacing range of 1.6m to 3.4m was used. This represents approximately 4 to 8 times the total pavement thickness. However, no through-thickness seismic wave data, even at the smallest spacing (1.6 m), were detected despite the large dynamic wave energy imparted by the gun source. It appears that the asphalt concrete material is dissipative of wave energy to the extent that the signal could not be detected at the

applied distances. However, some impact-echo frequency data at all testing locations were obtained. The obtained frequencies ranged from 3.7 kHz to 3.9 kHz. The spectrum at the peak was quite broad in shape, which also indicates a dissipative material. The obtained frequency corresponds to a P-wave velocity of 3000 to 3200 m/s, which is reasonable for this material.

For the 255mm thick pavement section, source receiver spacing range of 1.1m to 2.0 m was used. While some seismic data at the nearest sensor spacings can be obtained, the data from the far sensors was noisy and of dubious quality and usefulness. At farther sensor spacings no useful data was obtained. This is again likely caused by the dissipative nature of asphalt concrete to propagating wave energy. Moreover, no repeatable and reasonable impact-echo data from this test location could be obtained. The inability to collect impact-echo data may arise from the fact that this pavement section rests on lime-stabilized base, which is relatively stiffer than the granular base under the thicken AC pavement test section. This increased stiffness may result in low amplitude reflection echoes from the interface, similar to what was observed for portland cement concrete pavement atop asphalt-modified base.

Field Tests (Virginia)

The developed testing systems were evaluated on newly constructed pavements at two different locations in Virginia on August 16 and 17, 2005. At each location, the thickness predictions are compared to actual values obtained directly from drawn cores. The in-place strength predictions are compared to MOR values are obtained from VDOT from companion samples drawn from the same batch of concrete cast at that location.

Site Descriptions

Hampton

The NDT tests were carried out on August 16, 2005 at I-64, SOV4, STA 129+44 in Hampton, VA near the Mercury Blvd. (#263) exit. This section of pavement was cast on June 1, 2005, so the age of the concrete was 76 days at the time of testing. The weather at the time of test was sunny and warm. The nominal design of the pavement at this location is 280mm thick CRCP atop 75mm layer of asphalt-treated open-graded drainage layer, which is over a 150mm layer of cement-treated aggregate. The required design concrete 28-day compressive strength is 20.7 MPa (3000psi). The concrete contains crushed granite coarse aggregate and fly ash. The surface of the pavement is tined and treated with a curing compound. A core sample drawn from the test location on August 17, 2005 shows an average concrete slab depth of 314mm. The bottom surface of the core is uneven, showing significant bonding to the underlying base material.

Amherst

The NDT tests were carried out on August 17, 2005 at US 29 southbound, STA 495+50 south of Amherst, VA. This section of pavement was cast on August 10, 2005, so the age of the concrete was 7 days at the time of testing. The weather at the time of test was partly sunny and warm. The nominal design of the pavement at this location is 300mm thick CRCP atop 75mm thick asphalt concrete base course type BM-25, which is over a 200mm layer of cement-treated soil sub-base. The required design concrete 28-day compressive strength is 20.7 MPa (3000psi). The concrete contains crushed granite coarse aggregate and fly ash. The surface of the pavement is randomly tined. A core sample drawn from the test location on August 17, 2005 shows an average concrete slab depth of 306mm. The bottom surface of the core is flat and clean, and not bonded to the underlying base material.

Thickness Test Results

The pavement structures at both test locations were problematic for the thickness tests: it was very difficult or impossible to identify the mode converted P-S wave reflections from the bottom of the slab in the seismic time domain signals. A typical seismic time domain signal from the Hampton site is shown in Fig. 40b. For comparison, a typical seismic time domain signal from a concrete slab over granular base using a similar testing configuration is shown in Fig. 40a. For the seismic method, the arrival of multiply reflected mode converted waves prior to the surface wave must be identified. These echoes can be seen in signals collected from a slab over granular base (Fig 40a), but not in the signals from the Hampton test site (Figure 40b). The same problems were encountered at the Amherst test site. Usable impact-echo data also could not be obtained from the test site pavements. The impact-echo frequency data are dominated by a relatively low resonance frequency, and the expected impact-echo resonance for the concrete slab (5-7 kHz in these cases) is not observed. Thus no nondestructive test method estimates for thickness could be made.

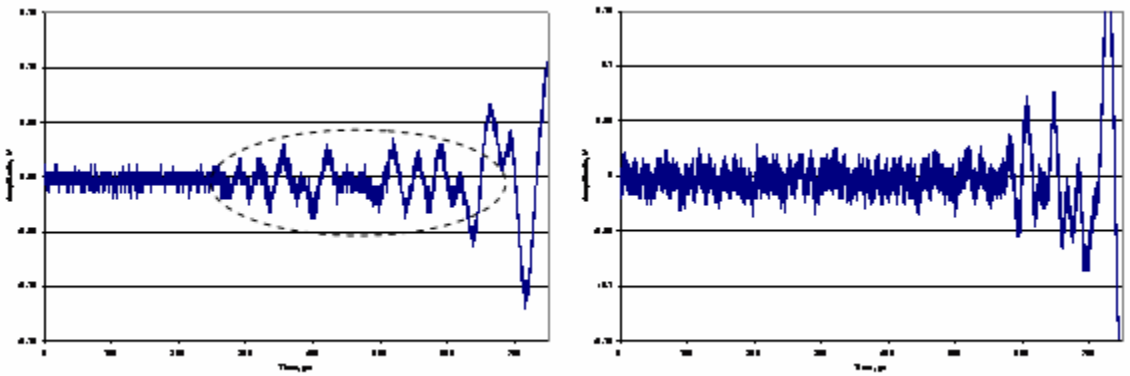

Figure 40: Typical seismic time domain signals obtained from (a) concrete pavement test slab over granular base and (b) concrete pavement at Hampton Virginia test site. The dashed circle indicates the region where mode converted P-S wave pulse arrive.

It is most likely that this problem is cased by the relatively stiff base material (asphalt concrete) immediately under the concrete slab. When a mechanical wave impinges on an interface between two materials, part of the incident energy is reflects and the rest is transmitted. The relative amount of reflected and transmitted energies depends on the relative "acoustic impedances" of the two materials, where the acoustic impedance is defined by the stiffness and density of the material. An interface between two materials that have similar stiffness and density (for example, PCC and asphalt concrete) will reflect relatively little wave energy, thus most of the energy is transmitted in to the asphalt concrete layer and little is reflected back to the receiver. An interface between concrete and granular base would reflect much more wave energy, enabling the reflections to be detected in the seismic and impact echo methods.

To confirm this speculation, additional subsequent seismic and impact-echo tests were carried out at pavement test sites at the ATREL pavement test facility of the University of Illinois. The tests were applied to two sections of concrete pavement: one over granular base and the other over an asphalt concrete base. The concrete slabs were comparable in terms of thickness and material properties. Useful seismic and impact-echo data from the slab atop granular base were collected. However, no useful data from the slab over asphalt concrete base were obtainable. This proves that the higher stiffness associated with asphalt-stabilized and asphalt concrete bases under concrete result in very little wave reflection at the interface between the two, rendering the seismic and impact-echo methods unusable in that case.

Strength Test Results

Hampton

Because of unexpected contractor-related issues, no concrete paving took place in Hampton in the weeks before the site visit there. As a result, no new (within 28 days after casting) pavements were available for testing during the visit. Furthermore, no in-place strength data for the concrete mixtures were available because of a misunderstanding with the local site engineer. Nevertheless, ultrasonic tests were carried out at the Hampton site on mature concrete (76 days old), and a prediction of in-place flexural strength was made based on those data. Since 1-day ultrasonic and strength values were unavailable, the second strength estimation approach was applied. The following ultrasonic parameters were obtained; T100 = 0.3419 and T220 = 0.2220. Application of Eqn. 22 shows the ratio T220/ T100 lies above the line. Thus Eqn. 19 was used to compute strength, where the predicted in-place MOR is 689.9 psi. This value is reasonable for mature normal-strength concrete, but the accuracy of this prediction could not be verified.

Amherst

Ultrasonic test at Amherst were carried out after seven days of casting. Since 1-day ultrasonic and strength values were unavailable, the second strength estimation approach again was applied. The following ultrasonic parameters were obtained; T100 = 0.2529 and T220 = 0.2010. Application of Eqn. 22 shows the ratio T220/ T100 lies above the line. Thus Eqn. 19 was used to compute strength, where the predicted in-place MOR is 528.1 psi. The measured 7-day MOR value for that concrete batch (provided by site engineer) was of 530psi. The strength

estimate error for this single point is approximately 2 psi. In this case, the two step approach provided an excellent prediction of in-place MOR.

DISCUSSION

Pavement Thickness Determination

Differences and errors observed encountered in the thickness prediction work are discussed here.

Usable hybrid method and impact-echo data also could not be obtained from concrete pavements immediately over an asphalt concrete layer. It is most likely that this problem is cased by the similar acoustic impedances (stiffness) of asphalt concrete and portland cement concrete. An interface between two materials that have similar stiffness and density (for example portland cement concrete and asphalt concrete) will reflect relatively little wave energy, thus most of the energy is transmitted in to the asphalt concrete layer and little is reflected back to the receiver. An interface between concrete and granular base would reflect much more wave energy, enabling the reflections to be detected in the seismic and impact echo methods. The hybrid method and impact-echo also cannot be applied effectively to full-depth asphalt concrete pavement. This is likely caused by the extremely dissipative nature of asphalt concrete to propagating mechanical wave energy.

In the impact echo-method, it is reasonable to assume that underestimation of C_p by the one-sided method occurs and is caused by material property gradients through the thickness of the slab, since this method interrogates primarily the top section of the concrete. This gradient is caused by aggregate settlement and bleeding in early-age concrete, leaving the upper portion of the slab with lower aggregate content. It has been shown that moisture content variations (Popovics et al. 1998) and surface deterioration mechanisms such as sulfate attack may also establish wave velocity gradients with respect to slab depth (Boyd and Ferraro 2005); those effects were not considered here since new pavement were considered. The aggregate settlement should cause an increase in material wave velocity from top to bottom. The one-sided measurements are likely more affected by material property gradients than through-thickness measurements: in this case C_p measured along the surface would likely under-estimate through thickness velocity when a gradient caused by aggregate settlement exists.

It is known that the measured apparent wave velocity can be disrupted by inaccuracies in determining the precise moment of wave arrival (Popovics et al. 1998). The level of disruption is controlled by the type of wave source, type of detection sensor and wave arrival determination algorithm applied in the analysis, and manifests itself as changes in the average and variance of velocity data. Also the accuracy of the conventional impact-echo method is limited by the systematic error of the data collection system, which is controlled by signal acquisition parameters such as number of points and the sample interval in the digital signal. The user must be familiar with this systematic error limitation in order to apply the method properly.

It is clear that accuracy in the measurement is important. The new hybrid method requires accurate sensor spacing distance determination to correctly apply the method. A

recommended default value for sensor spacing is 50cm in order to minimize the effects of inaccurate sensor spacing measurement. Smaller spacing values can be used if desired, however spacing values less than 10cm may result in significant measurement error. To apply the new hybrid method, source receiver spacing in the range of 4 to 8 times the pavement thickness must be applied. Thus the user must have an a priori estimate (accurate within several inches) of the slab thickness in order to properly apply the method.

In-place Strength Determination

Differences and errors observed encountered in the in-place strength prediction work are discussed here. The analysis is divided into three parts: (i) effects possibly caused by material properties, (ii) effects caused by the construction and geometry of specimens, (iii) and effects possibly associated with the measurements themselves. Recommendations for testing are then given based on the analysis.

As discussed previously, material gradients within concrete slabs can exist, for example due to aggregate settlement. This could explain the differences observed in both surface wave velocity and transmission measurements between the upper (trowelled) and lower (form) surfaces. This settlement would arguably result in higher velocities and transmission on the bottom surfaces. The approach described in this study is however oriented towards field use on an existing pavement. In this case access to the bottom surface is not available. Surface finishing processes could also cause variation in the surface properties. This may explain differences between results obtained from slabs and beams. Slab specimens require more finishing effort, conceivably causing more significant material gradients.

It was noted that the fresh concrete workability properties played an important role in the quality of beams, cylinders, and slabs produced. The harsh nature of mixtures produced with trap rock required more compaction effort for these mixtures, even though the slump values were comparable to the limestone mixtures. This could explain the unexpected observation that aggregate type had the most significant impact on the strength values.

Ultrasonic surface wave measurement could be susceptible to the effects of nearby edge or joint boundaries or the geometrical properties of the specimens. To minimize the effects of these problems, it is recommended that tests should be performed away (at least 10cm) from any edge or joint in a pavement.

It is clear that accuracy in the measurement is important. Transmission and surface wave velocity measurements require accurate sensor spacing distance determination to correctly apply the methods. In the preliminary tests, coupling and orientation of the source were discovered to be important. When using an ultrasonic point transducer, such as the one described in the latter set of strength prediction experiments, attention should be given to maintain the sensor perpendicular to the surface with constant applied pressure applied.

CONCLUSIONS

- The developed hybrid seismic/impact-echo method provides on average estimates of concrete pavement within an accuracy of ±6 mm or better when pavement structure conditions permit. Applicable pavement structures are limited to steel-reinforced or plain concrete slabs atop grade or unbound granular base, regardless of surface tining conditions or presence of reasonable amount and sizes of internal defects. The method can be applied with confidence in those cases. Concrete pavements atop asphalt concrete or asphalt-stabilized granular material cannot be inspected with either the hybrid or impact-echo methods. The applicability of the methods to concrete slabs directly atop cement or lime-stabilized granular material is undetermined. Full-depth asphalt concrete pavements cannot be inspected with either the hybrid method or impact-echo method.

- The accuracy of the impact-echo method for thickness estimation is improved with a complete understanding of the phenomenon presented in this study. The impact-echo frequency characterized by the zero-group velocity point of the S1 lamb mode in the slab or layered system. Complete knowledge of this behavior allows thorough study of the nature of the impact-echo phenomenon. The effects of slab size, base stiffness and higher-order modes on the impact-echo frequency are established.

- The accuracy of the impact-echo method for thickness estimation is further improved by making the one-sided P-wave velocity measurement more robust and repeatable.

- Ultrasonic surface wave velocity and transmission measurements can be carried out reliably on concrete slabs, and the values correlate to concrete compressive and flexural strengths.

- Two approaches to predict in-place strength from ultrasonic surface wave measurements were developed. The in-place modulus of rupture of concrete can, on average, be estimated within ±50 psi, regardless of aggregate type and content, using transmission measurements and knowing values of strength and transmission for the same location at the age of 1 day. This first approach can be applied with confidence when 1-day data are available. If 1-day data are not available, the second approach can be applied. Combined surface wave transmission data give estimates of modulus of rupture regardless of aggregate type and content, but at a reduced accuracy; modulus of rupture can on average be estimated within approximately ±100 psi. If the concrete contains a single known type of coarse aggregate, the accuracy of strength prediction improves dramatically with application of the appropriate strength relation. The second approach can be applied with confidence in those cases.

- Surface wave velocity and transmission data can be collected from pavements regardless of surface tining condition, steel reinforcement configuration, slab thickness and base type.

RECOMMENDATION

- VDOT's Non-Destructive Testing Division should consider using ultrasonic surface wave velocity and transmission measurements on concrete slabs to estimate the in-place modulus of rupture.

BENEFITS AND COSTS ASSESSMENT

It is intended for this investigation to result in the development of two new nondestructive methods that can replace the current destructive methods, which require extraction of core samples from newly constructed concrete highways. The developed method for thickness estimation is not applicable to the rigid pavement design typically used in Virginia. The developed method for in-place strength estimation is applicable. Nevertheless, the benefits resulting in general from successful methods would be substantial and are not limited to the following:

- Being nondestructive, these methods will enable important quality-assurance inspections to be performed without introducing discontinuities in the new pavements that the current methods bring, thereby undoubtedly leading to longer lasting pavements.

- In addition, the time required to make the measurements involved in these new NDE methods is expected to be only minutes. At such a rate, and being non-destructive, more sampling locations can be evaluated, which would enable statistically relevant analysis and make such inspection as thorough as it has ever been.

- Since such inspection is the basis for determining the extent of contractor's compliance with construction specifications and, therefore, the percentage of bid price to be paid to the contractor at the end of the construction, these above two advantages would ensure that VDOT really receive what it has paid for.

- Since the overall cost of using these new NDE methods is expected to be extremely low, in comparison to the current cost of $500 per 4-lane mile for coring, the savings will be substantial.

- Being applicable also to existing concrete pavements, these NDE methods will also provide evaluation data that will be valuable for future rehabilitation of those pavements.

A user's manual was prepared to facilitate implementation of these methods in the pavements inspection program of the Virginia Department of Transportation and to bring these benefits to fruition. This manual describes in detail: (1) the electronic and transducer equipment required to perform the two different measurements, (2) diagrams of the setups of the equipment, and (3) the procedures for conducting these measurements.

It is envisioned by these investigators that, as a follow-up to this project, some sort of a prototype self-contained instrument that integrates all the components necessary for performing the two different nondestructive measurements will eventually be developed – likely with the cooperation of a reputable instrument maker. Such an instrument will further facilitate the implementation of these methods, where appropriate, in the rest of the country.

ACKNOWLEDGMENTS

The principal investigator acknowledges the significant contributions of the following persons to the work in this project: Alex Gibson, Gonzalo Gallo, Michael Haas, Anja Glusic, Jinying Zhu, Joni Ranchero, and Nicole Jackson.

REFERENCES

Achenbach, J.D. *Wave propagation in elastic solids*. Elsevier Science Publishers, Amsterdam, 1973.

American Concrete Institute. *In-place Methods to Estimate Concrete Strength*. *Report ACI 228.1R*, American Concrete Institute, Farmington Hills, MI, 2003.

American Concrete Institute. *Nondestructive Test Methods for Evaluation of Concrete Structures*. *Report ACI 228.2R*, American Concrete Institute, Farmington Hills, MI, 1998.

Boyd, A.J. and Ferraro, C.C. Effect of curing and deterioration on stress wave velocities in concrete, *ASCE Journal of Materials in Civil Engineering*, Vol. 17, No. 2, pp. 153-158, 2005.

Bray, D., and Stanley, R. *Nondestructive evaluation: A tool in design, manufacturing, and service.* CRC Press Inc, Boca Raton, FL, 1997.

Cho, Y. Non-destructive testing of high strength concrete using spectral analysis of surface waves, *NDT&E International,* Vol. 36, pp. 229-235, 2003.

Clemeña, G. *Use of the impact-echo method in non-destructive measurements of the thickness of new concrete pavements, Report FHWA/VA-45-R10*. Virginia Department of Transportation, Richmond, 1995.

Clemeña, G.G. Use of Impact-Echo Method in Nondestructive Measurement of the Thickness of New Concrete Pavements, *Structural Materials Technology – an NDT Conference*, ed. R.J. Scancella and M.E. Callahan, Technomic Publishing Inc., Lancaster PA, 1994.

Clemeña, G.G., and Steele, R.E. *Measurements of the Thickness of In-Place Concrete with Microwave Reflection. Report No. VTRC-88-R16*, Virginia Transportation Research Council, Charlottesville, 1988.

Develogic Corporation. *Equipment specifications.* http://www.develogic.com/eng .Accessed June 2003.

Ditri, J.J., Pilarski, A., Pavlakovic, B., Rose J.L. Generation of Guided Waves in a Plate by Axisymmetric Normal Surface Loading, *Proc. Review in Progress in Quantitative Nondestructive Evaluation,* Vol. 13, Plenum Press, New York, 1994.

Ewing, W.M., Jardetzky, W.S., and Press, F. *Elastic Waves in Layered Media,* McGraw-Hill Book Company, 1957.

Gallo, G. and Popovics, J.S. One-Sided Stress Wave Velocity Measurement in Concrete, *Journal of Advanced Concrete Technology*, Vol. 3, No. 3, pp.355-362, 2005.

Gibson, A. *Advances in nondestructive testing of concrete pavements*, Ph.D. Thesis, The University of Illinois, Urbana, IL, 2005.

Gibson, A. and Popovics, J.S. Lamb wave basis for impact-echo method analysis, *ASCE Journal of Engineering Mechanics*, Vol. 131, No. 4, pp. 438-443, 2005.

Graveen, C. *Nondestructive test methods to assess pavement quality for use in a performance-related specification*, M.S. Thesis, Purdue University, West Lafayette, IN, 2001.

Holland, S.D., Chimenti, D.E. Air-Coupled Acoustic Imaging with Zero-Group-Velocity Lamb Modes, *Applied Physics Letters*, Vol. 83 No. 13, 2003.

Indiana Department of Transportation (IDOT). *2006 Standards Specifications*, Section 501: Quality control/quality assurance, Portland cement concrete pavement, 2005.

Jones, R. *Non-destructive Testing of Concrete*. Cambridge University Press, London, 1962.

Kolluru, S.V., Popovics, J.S., Shah, S.P. Determining Elastic Properties of Concrete Using Vibrational Resonance Frequencies of Standard Test Cylinders, C*ement, Concrete, and Aggregates*, Vol. 22, No. 2, pp. 81–89, 2000.

Kosmatka, S.H., and Panarese, W.C. *Design and control of concrete mixtures.* Portland Cement Association, Skokie, Illinois, 4th Edition, 1994.

Mindness, S; Young, F, and Darwin, D. *Concrete*. Prentice Hall, Englewood Cliffs, NJ, 2003.

Popovics, J.S., Song, W., Ghandehari, M., Subramaniam, K., Achenbach, J.D. and Shah, S.P. Application of Surface Wave Transmission Measurements for Crack Depth Determination in Concrete, *ACI Materials Journal*, Vol.97, No.2, pp.127-135, 2000.

Popovics, J.S., Song, W., Achenbach, J.D., Lee, J.H., and Andre, R.F. One sided stress wave velocity measurement in concrete, *ASCE Journal of Engineering Mechanics*, Vol. 124, No. 12, pp. 1346-1353, 1998.

Popovics, J.S. Effects of Poisson's Ratio on Impact-Echo Test Analysis, *ASCE Journal of Engineering Mechanics*, Vol. 123, No. 8, 1997.

Qixian, L. and Bungey, J.H. Using compression wave ultrasonic transducers to measure the velocity of surface waves and hence determine dynamic modulus of elasticity for concrete, *Construction and Building Materials*, Vol. 10, pp. 237-242, 1996.

Sansalone, M. Impact-Echo: the Complete Story. *ACI Structural Journal*, Vol. 94, No. 6, pp. 777-786, 1997.

Sansalone, M., and Streett, W. *Impact-Echo Nondestructive Evaluation of Concrete and Masonry.* Ithaca, NY: Bullbrier Press, 1997.

Song, W.; Popovics, J.; Aldrin, J.; and Shah, S. Measurement of surface wave transmission coefficient across surface-breaking cracks and notches in concrete, *Journal of Acoustical Society of America,* Vol. 113, pp. 717-725, 2002..

APPENDIX A: IMPLEMENTATION MANUAL

This manual is intended to facilitate implementation of the developed testing methods in the pavements inspection program of Virginia Department of Transportation and to bring these benefits to fruition. For both tasks, this manual describes in detail: (1) the electronic and transducer equipment required to perform all measurements, (2) block diagrams of the setups of the equipment, and (3) the procedures for conducting these measurements along with directions to interpret the acquired signals.

Task 1: Pavement Thickness Determination

Required Equipment

The following equipment are needed to carry out the tests: impactor (spring-driven BB gun), 4mm diameter spherical steel BBs, digital oscilloscope or other 2-channel DAQ system (8-bit digitizing with sample frequency at least 1 MHz) with associated field-worthy computer that contains developed analysis software, two accelerometers (sensitivity = 10.9mV/g @100 Hz and resonant frequency = 60 kHz) , two signal conditioning boxes (needed to bias accelerometers), tape measure, pencil/chalk, electric power source, impact-echo testing equipment (per ASTM C1383 standard).

Testing Configuration

Follow the following steps to set-up, configure and carry out the tests:

1. Connect near accelerometer in channel 1 of DAQ system and select location on concrete. Attach accelerometer to surface point with mounting wax. Ensure that all testing points are at least 10cm away from any edge or joint boundary.
2. Connect far accelerometer on channel 2 and attach to surface 20 to 50cm behind the first accelerometer, as shown in Figure A1, with mounting wax. If the pavement contains surface tining, place the sensors such that the line between them is parallel to the tining direction.
3. Estimate slab thickness (h). Then select 10 equally-spaced impact points which range in distance of 4h to 8h from the far accelerometer to impact.
4. Determine an appropriate range for time and amplitude in the DAQ system in order to capture the mode-converted P-S waves arriving before the large Raleigh surface wave for all impact locations on both channels.
5. Place the impact gun at the first location and fire. Ensure both signals look appropriate; i.e. mode-converted P-S wave arrivals are apparent. (see Figure A2) Save appropriate time signals to DAQ system.
6. Repeat procedure for all impact locations. Be sure to reset DAQ system before each impact and to save all time domain signal data.
7. Collect impact-echo frequencies, following the procedure in ASTM C1383-98, at several locations along the line and within the region between the impacts and sensors, including the two sensor locations. Report the average frequency from these tests.

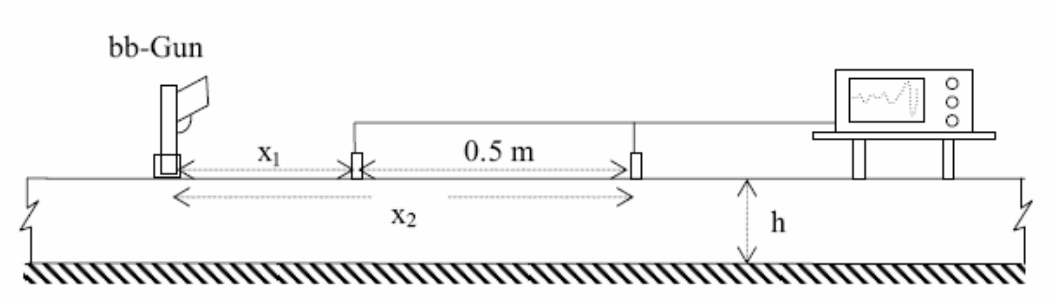

Figure A1: Data collection setup

Testing and Analysis Procedure

Carry out the following steps to analyze the collected data:

1. Retrieve the saved time domain signals and display them in amplitude vs. time plots.
2. In each signal determine, where possible, the arrival times of the direct P-waves and P-S and PP-SS wave pulses. Guidance for wave arrival determination is given in Figure A2. Note that PP-SS arrivals in channel 2 and P-S in channel 1 may occur after the Raleigh surface wave and can not be obtained visually.
3. Start up the developed seismic analysis computer program (Excel VBA format) and input the arrival times into the appropriate spaces. Be sure to use only positive time values: the delay setting on the DAQ system can cause negative values so in that case a constant time value must be added to all arrival times to bring the values to positive numbers. Any data that were unable to be determined, such as the PP-SS from smaller impact spacings or arrivals after Rayleigh wave, should be left blank.
4. After the data are input, click over to "fitting" page in the seismic analysis program, and input the average impact-echo frequency in the space provided.
5. Input an estimated shear wave velocity. The surface P-wave velocity, based in to the input data, is displayed on the screen. A good estimate for shear velocity is 60% of the P-wave velocity.
6. The program now displays a phase velocity dispersion curve for the pavement system. Each curve represents a different Poisson's ratio of the concrete. The data from the mode-converted P-S reflections appear as points, and the impact echo frequency is displayed as a single vertical line. (see Figures A3 and A4)
7. In an iterative fashion, apply the toggle switches for varying pavement thickness and Poisson's ratio until the Impact Echo frequency becomes tangent with left most point of that dispersion curve most closely associated with the data points.
8. The thickness value and Poisson's ratio that gives best fit to the points (mode converted echoes) and vertical line (impact-echo) are the final estimates for the slab.

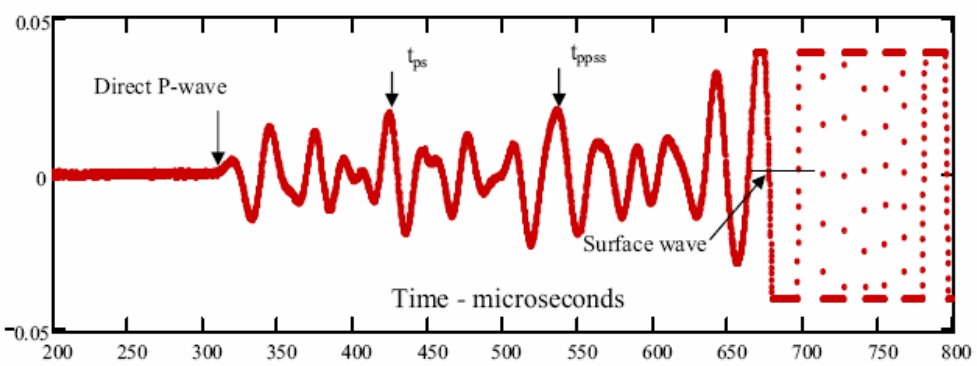

Figure A2: Typical wave signal from BB impact

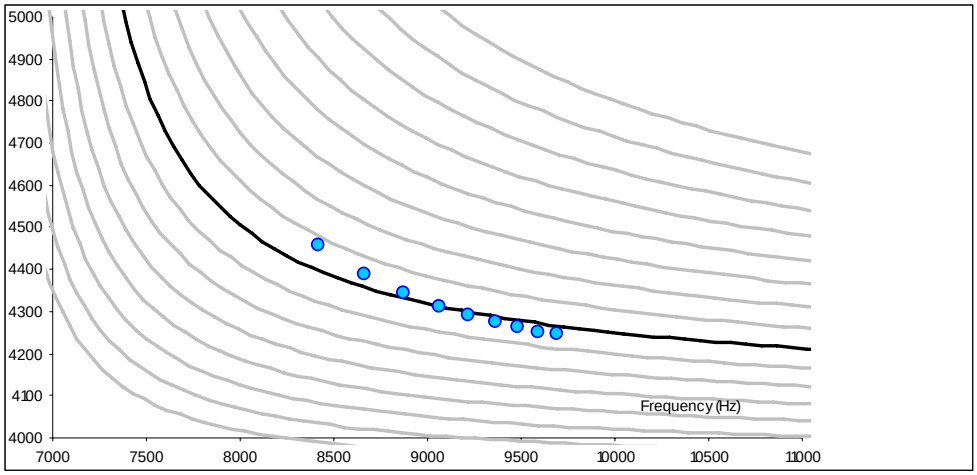

Figure A3: Zoom-in of phase velocity vs. frequency graphs for varying Poisson's ratio (colored lines). Mode-converted P-S wave arrivals (points) align with appropriate dispersion curve

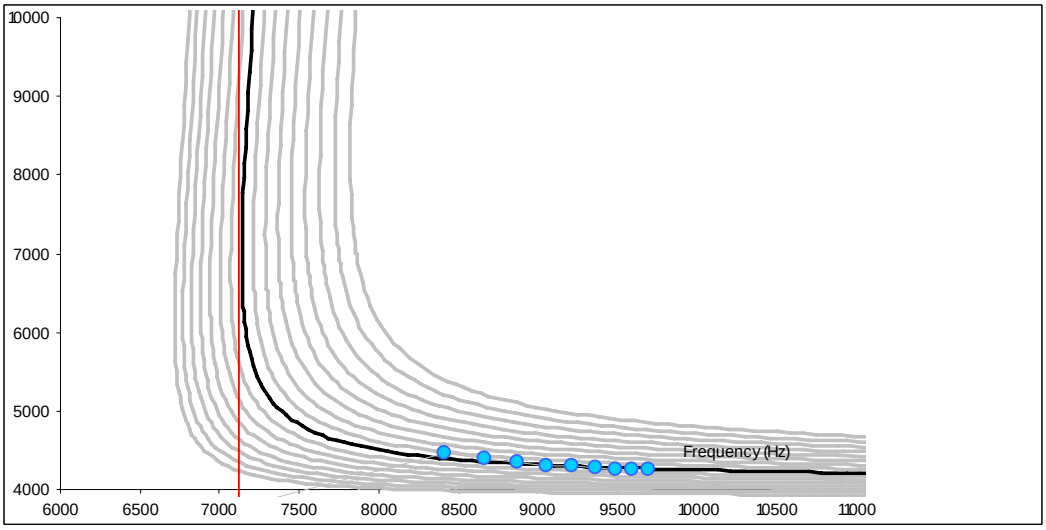

Figure A4: Phase velocity vs. frequency graphs very varying Poisson's ratio (colored lines) with showing mode-converted P-S wave arrivals (points) and impact-echo frequency (vertical line).

Task 2: In-place Strength Determination

This guide serves to instruct the procedure and analysis needed to determine surface wave velocity and surface wave transmission from field tests.

Required Equipment

The following equipment are needed to carry out the tests: ultrasonic pulser unit and associated high frequency (above 100 kHz) surface wave exponential transducer with point excitation (see Figure A6), digital oscilloscope or other DAQ system (8-bit digitizing with sample frequency at least 1 MHz) with associated field-worthy computer that contains developed analysis software, two accelerometers (sensitivity = 10.9mV/g @100 Hz and resonant frequency = 60 kHz) , two signal conditioning boxes (needed to bias accelerometers), tape measure, pencil/chalk, and electric power source.

Testing Configuration

Follow the following steps to set-up, configure and carry out the tests.

Surface wave velocity

1. Connect near accelerometer to channel 1 of DAQ system and far accelerometer to channel 2. The accelerometers are surface-mounted to the concrete along a line at a separation distance of 2 cm. Select a testing location where there are no apparent surface damage such as voids and that is generally smooth and flat. Ensure that all testing points are at least 10cm away from any edge or joint boundary.
2. Place point transducer along line defined by accelerometers 2 cm away from the near accelerometer. If the pavement contains surface tining, place the sensors such that the line between them is parallel to the tining direction. Activate the ultrasonic pulser and collect 50 data from both sensors. Time average the 50 signals to give one averaged (lower signal to noise ratio) from each sensor. Save the averaged time signals to the DAQ system.
3. Move the ultrasonic transducer and near sensor to new a new location 1 cm away from the previous. Maintain a 2 cm spacing between transducer and near sensor. (see Figure A5) Measure spacing between the sensors. Activate ultrasonic pulse and collect two averages signals as described in step 2.
4. Repeat step 3 multiple times until a set of 6 spacings between sensors is obtained.

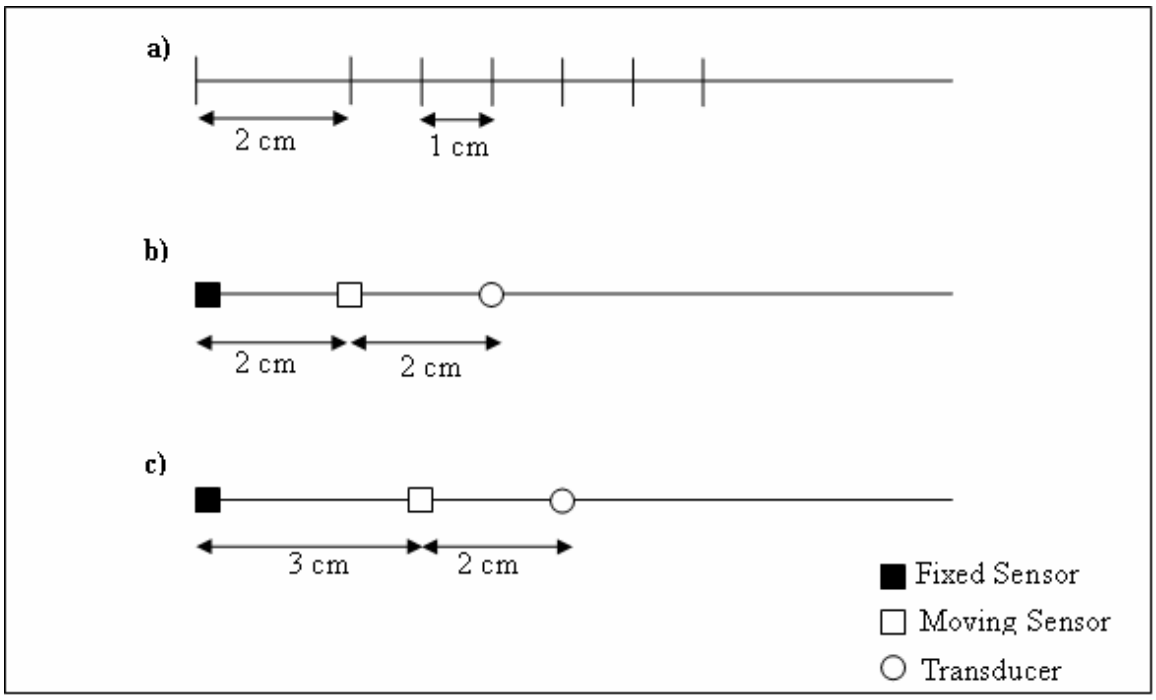

Figure A5: Plan view of placing procedure of sensors and transducer for surface wave velocity measurements

Figure A6: (a) Ultrasonic Pulser Unit (V-Meter) and (b) ultrasonic surface wave transducers

Surface wave transmission

1. Connect one accelerometer to channel 1 of DAQ system and the other accelerometer to channel 2. The accelerometers are surface-mounted to the concrete along a line at a separation distance of 7 cm (locations "2" and "3" in Figure A7). Select a testing location where there are no apparent surface damage such as voids and that is generally smooth and flat. Ensure that all testing points are at least 10cm away from any edge or joint boundary.

2. Place point transducer along line defined by accelerometers 7 cm away from the channel 1 accelerometer. (location "1" in Figure A7) A positioning frame was used to keep sensors and transducer at the desired location to assure the spacing is maintained and also to enable faster measurements.
3. Activate the ultrasonic pulser and collect 50 data from both sensors using a time signal duration of 200 μs. Ensure that the gain setting of the DAQ system are suitable so to collect the entire signal without clipping or saturation. Time average the 50 signals to give one averaged (lower signal to noise ratio) from each sensor. Collect 5 separate sets of averaged data and save the time signals to the DAQ system.
4. Move the ultrasonic transducer to the opposite side of the sensors pair and place on the surface 7cm away from channel 2 sensor. (location "4" in Figure A7) Activate ultrasonic pulse and collect two averages signals as described in step 3.

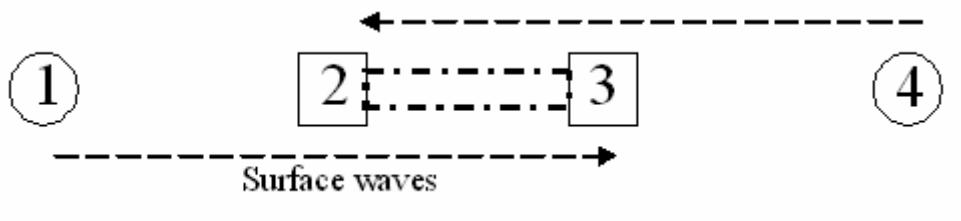

Figure A7: Sketch (plan view) of self-compensating wave transmission testing configuration. The circles represent wave sources and the squares wave receivers.

Testing and Analysis Procedure

Carry out the following steps to analyze the collected data:

Surface wave velocity

1. Retrieve the saved time domain signals and display them in amplitude vs. time plots.
2. In each signal determine the arrival time of the Rayleigh wave pulse. A common defining feature of the signals must be defined do to this: the most reliable signal feature is either the first significant peak or valley.
3. Once the arrival times have been recorded for all the locations, plot the time difference of the signal arrival between the two sensors against the distance between them and determine the best -fit line through the data. Table A1 gives guidance in this regard. The slope of the equation of the curve is the surface wave velocity.

Table A1: Example of table with data used for surface wave velocity determination

Sensor separation (*i*)	$S_{1,i}$	$S_{2,i}$	$\Delta t_i = (S_{2,i} - S_{1,i})$
cm	μs	μs	μs
2	$S_{1,2}$	$S_{2,2}$	$\Delta t_2 = (S_{2,2} - S_{1,2})$
3	$S_{1,3}$	$S_{2,3}$	$\Delta t_3 = (S_{2,3} - S_{1,3})$
4	$S_{1,4}$	$S_{2,4}$	$\Delta t_4 = (S_{2,4} - S_{1,4})$
5	$S_{1,5}$	$S_{2,5}$	$\Delta t_5 = (S_{2,5} - S_{1,5})$
6	$S_{1,6}$	$S_{2,6}$	$\Delta t_6 = (S_{2,6} - S_{1,6})$

Surface wave transmission

1. Start up the developed surface wave transmission computer program (Executable file format coded in LabWindows environment). See Figure A8.
2. Extract desired time signals with "Acquire" button. Using the movable cursors identify the first significant peaks or valleys of each signal, which indicate the arrival of the Rayleigh surface waves and serve to center the time signal for windowing processing.
3. Once the 10 averaged signals are loaded, press the "Analysis" button and the final transmission signal and coherence functions are plotted. Store this signal using the "Save Result" button. The program carries out all necessary signal processing, FFTs and manipulation (described earlier in this report) that are required by the procedure.
4. Extract the transmission values at 100kHz and 220kHz with a coherency above 0.99.
5. If 1 day values are available for MOR estimation, input the transmission values at 220kHz into equation 20.
6. If the 1 day values are not available, input transmission values into equation 21 and compare the output to the ratio of measured transmissions. If the measured ratio is higher than the value from the equation, use equation 18. Otherwise, use equation 19 for MOR prediction.

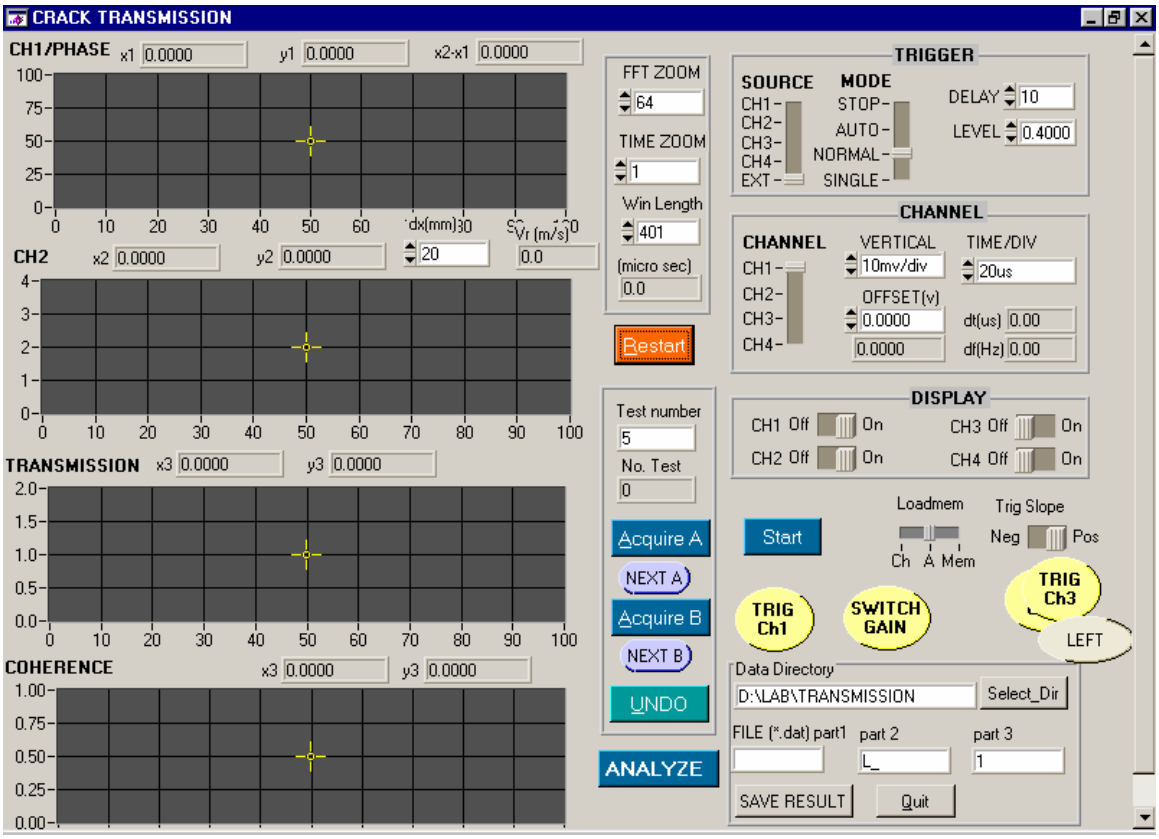

Figure A8: Screenshot of the surface wave transmission program user interface

APPENDIX B: LIST OF SYMBOLS

The following symbols are used in the text of the report.

Symbols and Definition	Default Units
A = antisymmetrical solution mode	
a = projection of reflection	m
C_G = group velocity	m/s
C_p = primary wave velocity	m/s
C_{ph} = phase velocity	m/s
C_s = shear wave velocity	m/s
d_{ij} = transmission between i and j	
F = experimental frequency	Hz
fc = compressive strength	MPa
$f'c_{i\text{-}measured}$ = actual compressive strength	MPa
$f'c_{i\text{-}predicted}$ = predicted compressive strength	MPa
h = slab thickness	m
k = wavenumber	1/m
L = length of FEM model	m
n = total number of data points	
R_i = receiving response term	
S = symmetrical solution mode	
SC = signal consistency function	
S_i = generating response term	
S_1 = first-order symmetric Lamb mode	
T_R = surface wave transmission	m/s
V_{ij} = Fourier transformed signal	
x_i = horizontal distance	m
X_P = theoretical ray-paths of P waves	m
X_S = theoretical ray-paths of S waves	m
Z = acoustic impedance	kg/(m^{2}s)
Ω = normalized frequency	
β = Impact Echo correction factor	
Δt = time from near to far sensor	s
ΔV = velocity systematic error	m/s
K = C_p / C_s	
ν = Poisson's ratio	
ξ = normalized wave-number	
ρ = mass density	kg/m^3
ω = circular frequency	kg/m3
θ_P = P wave angle	degrees or radians
θ_s = S wave angle	degrees or radians